Thermodynamically compatible discretization of a compressible two-fluid model with two entropy inequalities

Andrea Thomann, Michael Dumbser

Noname manuscript No.
(will be inserted by the editor)

Thermodynamically compatible discretization of a compressible two-fluid model with two entropy inequalities

Andrea Thomann · Michael Dumbser

Received: date / Accepted: date

Abstract We present two methods for the numerical solution of an overdetermined symmetric hyperbolic and thermodynamically compatible (SHTC) model of compressible two-phase flows which has the peculiar feature that it is endowed with *two entropy inequalities* as primary evolution equations. The total energy conservation law is an extra conservation law and is obtained via suitable linear combination of all other equations based on the Godunov variables (main field). In the stiff relaxation limit the SHTC model tends to an asymptotically reduced Baer-Nunziato-type (BN) limit system with a unique choice for the interface velocity and the interface pressure, including parabolic heat conduction terms and additional lift forces that are not present in standard BN models. Both numerical schemes directly discretize the two entropy inequalities, including the entropy production terms, and obtain total energy conservation as a consequence. The first method is of the finite volume type and makes use of a thermodynamically compatible flux recently introduced by Abgrall *et al.* that allows to fulfill an additional extra conservation law exactly at the discrete level. The scheme satisfies both entropy inequalities by construction and can be proven to be nonlinearly stable in the energy norm. The second scheme is a general purpose discontinuous Galerkin method that achieves thermodynamic compatibility merely via the direct solution of the underlying viscous regularization of the governing equations. We show computational results for several benchmark problems in one and two space dimensions, comparing the two methods with each other and with numerical results obtained for the asymptotically reduced BN limit system. We also investigate the influence of the lift forces.

A. Thomann
Université de Strasbourg, CNRS, Inria, IRMA, Strasbourg F-67000, France
E-mail: andrea.thomann@inria.fr
M. Dumbser *
Department of Civil, Environmental and Mechanical Engineering, University of Trento, Via Mesiano 77, I-38123 Trento, Italy E-mail: michael.dumbser@unitn.it

Keywords thermodynamically compatible schemes, overdetermined hyperbolic systems with two entropy inequalities, thermodynamically compatible finite volume method, discontinuous Galerkin schemes, compressible multiphase flows

1 Introduction

Compressible two-phase flows are of fundamental importance in science and engineering. Potential applications range from geophysical multi-phase flows of solid-gas mixtures in avalanches and pyroclastic flows after volcano explosions to industrially relevant flows, from the injection of fuel droplets in internal combustion engines as well as turbo- and rocket engines in aerospace engineering over flows of gas-liquid and multi-fluid mixtures in food and paper industry up to multi-phase flows in nuclear power plants. At present, there is no universally accepted mathematical model for such flows and several different formulations can be found in the literature. Some of the most well-known models based on the diffuse interface approach, which does not require an explicit tracking of the material interface and its changing topology, include the Baer-Nunziato (BN) system of compressible multi-phase flows [13] and its stiff relaxation limit, the so-called Kapila model [52]. This kind of models have been extensively studied and applied, for example, in [11,12,70,67,6, 60,31,4,44,56,45,69,61,28,27]. The drawback of BN-type models is the presence of non-conservative terms, whose discretization may be non-trivial, see e.g. [54,24,58,40,25,5] for possible solutions and related problems. Two completely different mathematical descriptions of compressible multi-fluid flows are the Scannapieco-Cheng model [68], which is fully conservative, as well as the discrete equation model of Abgrall and Saurel [10], in which the discretization of non-conservative products can be avoided. We also would like to mention Navier-Stokes-Korteweg-type systems for the description of compressible multi-phase flows with phase transition, see e.g. [34,57,26,51,32,33]. Yet another class of diffuse interface models for compressible multi-phase flows can be found in recent work of Romenski *et al.* [66,65,64]. It is based on the theory of symmetric hyperbolic and thermodynamically compatible (SHTC) systems introduced by Godunov and Romenski [48,63,50] and was recently studied analytically and numerically for the barotropic case in [71,53]. In the more general non-barotropic case, the SHTC model is based on *two entropy inequalities* as primary evolution equations and *one scalar* extra conservation law, which is the total energy conservation equation for the mixture. From a numerical point of view, the non-batropic SHTC model poses a very interesting and extremely challenging problem. Usually, in numerical methods for hyperbolic conservation laws with applications to single phase flows, the scalar entropy balance law is simply *replaced* by the scalar total energy conservation law, which is then directly solved by the numerical scheme instead of the entropy balance. However, in models with two or more entropy inequalities opposing only one scalar energy conservation law, this is no longer possible,

since the arising multiple entropy inequalities cannot be substituted by one single scalar equation inside the numerical scheme.

To the best knowledge of the authors, the full non-barotropic SHTC model of compressible two-fluid flow proposed in [66,65,64] has never been solved numerically before since there are currently no numerical schemes available that are able to solve overdetermined hyperbolic systems with *more than one entropy inequality*. It is therefore the main objective of this paper to develop such schemes for the first time.

The rest of this paper is organized as follows. In Section 2 we present the SHTC model of compressible two-phase flow of Romenski *et al.* as well as the associated Baer-Nunziato limit system, which is obtained in certain stiff relaxation limits of the full SHTC model. A new thermodynamically compatible finite volume scheme based on the general framework of Abgrall *et al.* [2,7,8,3,18] is presented in Section 3. It solves the two entropy inequalities directly, thus satisfying both of them *by construction*. It furthermore achieves total energy conservation as a consequence of the thermodynamically compatible discretization of all other equations. This ensures nonlinear stability of the scheme in the energy norm. A high order accurate general purpose discontinuous Galerkin scheme is presented in Section 4. This method also discretizes the two entropy inequalities directly and achieves thermodynamic compatibility merely by directly solving the smooth vanishing viscosity regularization of the equations. Numerical experiments validating the theoretical results are presented in Section 5. A comparison between the two schemes is performed as well as the behavior of the SHTC model in the stiff thermal relaxation limit with respect to the BN type system is illustrated. The paper closes with some concluding remarks and an outlook to future research given in Section 6.

2 Governing equations

In this paper we study the compressible two-fluid model of Romenski *et al.* [66, 65] with *two entropy inequalities*. Furthermore, it consists of two velocities, two pressures and two temperatures. To express the equations we use upper indices to denote the phase number and lower indices to indicate the tensor and vector indices. Throughout this paper we assume the Einstein summation convention over two repeated indices. Accordingly α^1 denotes the volume fraction of phase one and α^2 the volume fraction of phase two under the condition $\alpha^1 + \alpha^2 = 1$. Further, to each phase $l = 1, 2$ is associated a density ρ^l, a velocity field $\mathbf{v}^l = (v_1^l, v_2^l, v_3^l)$, and the field of thermal impulses $\mathbf{j}^l = (j_1^l, j_2^l, j_3^l)$. Furthermore, each phase is equipped with an equation of state (EOS) which constitutes the relation between phase entropies s^l, specific internal energies $e^l = e^l(\rho^l, \mathbf{j}^l, s^l)$, phase pressures $p^l = p^l(\rho^l, s^l)$ and temperatures $T^l = T^l(\rho^l, s^l)$ are given. In particular it holds

$$p^l = (\rho^l)^2 \frac{\partial e^l}{\partial \rho^l} \quad \text{and} \quad T^l = \frac{\partial e^l}{\partial s^l}. \tag{1}$$

In the following, we consider an ideal gas law with

$$e^l(\rho^l, \mathbf{j}^l, s^l) = \frac{1}{\gamma^l - 1}(\rho^l)^{\gamma^l - 1} \exp\left(\frac{s^l}{c_v^l}\right) + \frac{A^l}{2} j_k^l j_k^l \tag{2}$$

where the contribution of the thermal impulses to the internal energy is modelled by $A^l = \rho^l \kappa^l / \tau$. Therein κ^l denotes the thermal conductivity coefficient and τ the heat flux relaxation time. From the phase state variables $(\alpha^l, \rho^l, \mathbf{v}^l, \mathbf{j}^l, s^l)$, the mixture quantities are defined as the mixture density $\rho = \alpha^1\rho^1 + \alpha^2\rho^2$, the phase concentrations $c^l = \alpha^l\rho^l/\rho$, the averaged velocity $\mathbf{v} = c^1\mathbf{v}^1 + c^2\mathbf{v}^2$, the relative velocity $\mathbf{w} = \mathbf{v}^1 - \mathbf{v}^2$ and the total entropy of the mixture $S = c^1 s^1 + c^2 s^2$. The governing equations for two-phase flows based on the ideal gas EOS (2) consist of flux terms (black), source terms (green) and vanishing viscosity regularization terms (blue). They read

$$\partial_t \alpha^1 + v_k \partial_k \alpha^1 - \partial_m \epsilon \partial_m \alpha^1 = 0 \tag{3a}$$

$$\partial_t(\alpha^1\rho^1) + \partial_k\left(\alpha^1\rho^1 v_k^1\right) - \partial_m \epsilon \partial_m \alpha^1\rho^1 = 0 \tag{3b}$$

$$\partial_t(\alpha^2\rho^2) + \partial_k\left(\alpha^2\rho^2 v_k^2\right) - \partial_m \epsilon \partial_m \alpha^2\rho^2 = 0 \tag{3c}$$

$$\partial_t(\rho v_i) + \partial_k\left(\rho v_i v_k + p\,\delta_{ik} + \rho w_i E_{w_k}\right) - \partial_m \epsilon \partial_m \rho v_i = 0 \tag{3d}$$

$$\partial_t w_k + \partial_k\left(v_m w_m + E_{c^1}\right) + v_i\left(\partial_i w_k - \partial_k w_i\right) - \partial_m \epsilon \partial_m w_k = -\frac{\lambda_k^0}{\rho} \tag{3e}$$

$$\partial_t(\rho j_i^1) + \partial_k\left(\rho j_i^1 v_k + \delta_{ik} T^1\right) - \partial_m \epsilon \partial_m \rho j_i^1 = -\lambda_k^1 \tag{3f}$$

$$\partial_t(\rho j_i^2) + \partial_k\left(\rho j_i^2 v_k + \delta_{ik} T^2\right) - \partial_m \epsilon \partial_m \rho j_i^2 = -\lambda_k^2 \tag{3g}$$

$$\partial_t(\alpha^1\rho^1 s^1) + \partial_k\left(\alpha^1\rho^1 s^1\, v_k + A^1 j_k^1\right) - \partial_m \epsilon \partial_m \alpha^1\rho^1 s^1 = \Pi_1 + \pi_1 \geq 0 \tag{3h}$$

$$\partial_t(\alpha^2\rho^2 s^2) + \partial_k\left(\alpha^2\rho^2 s^2\, v_k + A^2 j_k^2\right) - \partial_m \epsilon \partial_m \alpha^2\rho^2 s^2 = \Pi_2 + \pi_2 \geq 0 \tag{3i}$$

where E denotes the specific total energy of the system given by the sum of the specific internal energy, the kinetic energy of relative motion and the kinetic energy

$$E = c^l e^l(\rho^l, \mathbf{j}^l, s^l) + c^1 c^2 \frac{w_k w_k}{2} + \frac{v_k v_k}{2}. \tag{4}$$

The partial derivatives of E in the above given momentum and relative velocity equations in order of appearance can be obtained from (4) and are given by

$$E_{w_k} = c^1 c^2 w_k, \quad E_{c^1} = \mu^1 - \mu^2 + (1 - 2c^1)\frac{w_k w_k}{2}, \tag{5}$$

where μ^l denote the chemical potentials or Gibbs free energies

$$\mu^l = e^l + \frac{p^l}{\rho^l} - s^l T^l. \tag{6}$$

In addition to the above given governing equations (3), we obtain the total energy conservation law with $\mathcal{E} = \rho E$ from a linear combination of all governing equations (3) given by

$$\partial_t \mathcal{E} + \partial_k \left(v_k(\mathcal{E}+p) + \rho v_i w_i E_{w_k} + \rho E_c E_{w_k} + E_{j_k^1} T^1 + E_{j_k^2} T^2 \right) - \partial_m \epsilon \partial_m \mathcal{E} = 0. \quad (7)$$

Note, that the energy conservation law is obtained as a consequence and the two-fluid system (3) with (7) is overdetermined.

In the parabolic vanishing viscosity regularization terms (blue), the diffusion parameter ϵ is assumed to be non-negative. The individual phase entropy production terms that arise this parabolic regularization must be compatible with total energy conservation and are defined as

$$\Pi_l = \epsilon \frac{c^l}{T^l} \frac{\partial q_i}{\partial x_m} \partial^2_{q_i q_j} \mathcal{E} \frac{\partial q_j}{\partial x_m} \geq 0. \quad (8)$$

They are non-negative, since the concentrations $c^l \geq 0$ and the phase temperatures $T^l > 0$ are all non-negative. Moreover, we also assume the Hessian of the total energy potential $\partial^2_{q_i q_j} \mathcal{E}$ to be at least positive semi-definite.

To complete the description of the governing equations (3), we turn towards the source terms (green). They concern friction ζ and relaxation processes based on thermal conductivity and act on the relative velocity equations (3e), the thermal impulses (3f),(3g) and the entropies (3h), (3i). They are given by

$$\lambda^0_k = \chi^0 c^1 c^2 w_k + \chi^l c^l A^l j^l_k, \qquad \lambda^l_k = \chi^l c^1 c^2 w_k + \frac{1}{c^l \kappa^l} c^l A^l j^l_k \quad (9)$$

for relative velocity and thermal impulses. The phase entropy source terms π_l are non-negative and contribute to the entropy production as

$$\begin{aligned} \pi_l =& \frac{\chi^l}{T^l} \sum_k \left(c^l A^l j^l_k + \frac{\chi^l}{c^l \kappa^l} c^1 c^2 w_k \right)^2 \\ &+ \frac{c^l}{T^l} \left(\chi^0 - \frac{(\chi^1)^2}{c^1 \kappa^1} - \frac{(\chi^2)^2}{c^2 \kappa^2} \right) \sum_k (c^1 c^2 w_k)^2 \geq 0. \end{aligned} \quad (10)$$

To simplify notation, we use therein the auxiliary variables

$$\chi^l = (-1)^l \frac{\rho s^l}{c^l \kappa^l}, \quad \chi^0 = \zeta + \frac{(\chi^l)^2}{c^l \kappa^l}. \quad (11)$$

Note that model (3) also allows for a pressure relaxation source term in the evolution equation of the volume fraction (3a) as well as phase exchange terms in the partial density equations (3b),(3c), for details see [66,65]. They have been neglected in the description of the governing equations (3) since the work presented here focuses on the derivation of the numerical schemes for the flux terms (black) and the comparison of the two-fluid model with the asymptotically reduced BN-type model in the stiff relaxation limit $\kappa^l \to 0$ which is described in the next section.

2.1 Stiff relaxation limit: a Baer-Nunziato-Fourier-type system

In the stiff relaxation limit when $\kappa^l \to 0$ and for vanishing viscosity $\epsilon \to 0$ under zero inter-phase friction, the model can be shown to reduce to the following *non-conservative* parabolically regularized two-temperature Baer-Nunziato-type limit system

$$\partial_t \alpha^1 + v_k \partial_k \alpha^1 = 0 \tag{12a}$$
$$\partial_t \alpha^1 \rho^1 + \partial_k \left(\alpha^1 \rho^1 v_k^1 \right) = 0 \tag{12b}$$
$$\partial_t \alpha^2 \rho^2 + \partial_k \left(\alpha^2 \rho^2 v_k^2 \right) = 0 \tag{12c}$$
$$\partial_t \alpha^1 \rho^1 v_i^1 + \partial_k \left(\alpha^1 \rho^1 v_i^1 v_k^1 + \alpha^1 p^1 \, \delta_{ik} \right) + p^I \partial_i \alpha^1 - f_i = 0 \tag{12d}$$
$$\partial_t \alpha^2 \rho^2 v_i^2 + \partial_k \left(\alpha^2 \rho^2 v_i^2 v_k^2 + \alpha^2 p^2 \, \delta_{ik} \right) + p^I \partial_i \alpha^2 + f_i = 0 \tag{12e}$$
$$\partial_t \alpha^1 \rho^1 E^1 + \partial_k \left(v_k^1 (\alpha^1 \rho^1 E^1 + \alpha^1 p^1) - c^1 \kappa^1 T^1 \partial_k T^1 \right) + \beta_k^1 \partial_k \alpha^1 - v_k^1 f_k = 0 \tag{12f}$$
$$\partial_t \alpha^2 \rho^2 E^2 + \partial_k \left(v_k^2 (\alpha^2 \rho^2 E^2 + \alpha^2 p^2) - c^2 \kappa^2 T^2 \partial_k T^2 \right) + \beta_k^2 \partial_k \alpha^2 + v_k^2 f_k = 0 \tag{12g}$$

with the specific phase energies

$$E^l = e^l + \frac{u_i^l u_i^l}{2}. \tag{13}$$

The interface quantities p^I and u^I are a consequence of the stiff heat relaxation limit $\kappa^l \to 0$ and cannot be chosen arbitrarily. They are given by

$$p^I = c^1 p^2 + c^2 p^1, \quad v_k^I = c^1 v_k^1 + c^2 v_k^2 = v_k. \tag{14}$$

For details concerning their derivation, see [66,65]. Moreover, we have

$$\beta_k^m = -p^m v_k^I - (p^I - p^m) v_k^m. \tag{15}$$

A substantial difference between the SHTC model (3) and standard BN systems arises due to the appearance of the lift forces in multiple space dimensions

$$f_i = \rho c^1 c^2 w_k \left(c^1 \left(\frac{\partial v_i^2}{\partial x_k} - \frac{\partial v_k^2}{\partial x_i} \right) + c^2 \left(\frac{\partial u_i^1}{\partial x_k} - \frac{\partial u_k^1}{\partial x_i} \right) \right). \tag{16}$$

These terms appear as additional non-conservative terms in the limit BN system, due to the rotational term in the relative velocity equation of the SHTC model (3).

2.2 General formulation of the governing PDE system

Since the two fluid model (3) given above is just one example of a more general class of symmetric hyperbolic and thermodynamically compatible (SHTC) systems, see e.g. [63,50], we will employ a more general framework for the development of the numerical discretization. Examples are continuum mechanics,

magnetohydrodynamics or the turbulent shallow water model of Gavrilyuk *et al.* [42,49,47,20]. They take the following general form

$$\partial_t \mathbf{q} + \partial_k \mathbf{f}_k(\mathbf{q}) + \mathbf{B}_k(\mathbf{q})\partial_k \mathbf{q} - \partial_m \left(\epsilon \partial_m \mathbf{q}\right) = \mathbf{P}(\mathbf{q}, \nabla \mathbf{q}) + \mathbf{S}(\mathbf{q}), \tag{17}$$

with the extra conservation law for the total energy density

$$\frac{\partial \mathcal{E}}{\partial t} + \partial_k F_k - \partial_m \left(\epsilon \partial_m \mathcal{E}\right) = 0. \tag{18}$$

Therein, $\mathbf{q}$ is the state vector, the flux tensor is denoted by $\mathbf{f}_k(\mathbf{q})$ and $\mathbf{B}_k(\mathbf{q})\partial_k \mathbf{q}$ contains the non-conservative terms. The vanishing viscosity terms are given by $\partial_m \left(\epsilon \partial_m \mathbf{q}\right)$ with the associated entropy production term $\mathbf{P}$. If present in the model, the relaxation source terms are contained in $\mathbf{S}(\mathbf{q})$. In the extra conservation law (18) the total energy flux is denoted by $F_k = F_k(\mathbf{q})$.

The *main field* or *thermodynamic dual variables* are defined as $\mathbf{p} = \partial_{\mathbf{q}} \mathcal{E}$ and therefore it holds by chain rule $\mathbf{p} \cdot \partial_t \mathbf{q} = \partial_t \mathcal{E}$. Thus, to guarantee thermodynamic compatibility of the full system (17) with the energy conservation (18), the following identity must hold

$$\mathbf{p} \cdot \partial_k \mathbf{f}_k(\mathbf{q}) + \mathbf{p} \cdot \mathbf{B}_k(\mathbf{q})\partial_k \mathbf{q} = \partial_k F_k. \tag{19}$$

Moreover, we also have to ensure the compatibility of the dissipation terms with the production term $\mathbf{P}$ given by

$$\mathbf{p} \cdot \mathbf{P} + \mathbf{p} \cdot \partial_m \left(\epsilon \partial_m \mathbf{q}\right) = \partial_m \left(\epsilon \partial_m \mathcal{E}\right), \tag{20}$$

and the compatibility of the algebraic source terms

$$\mathbf{p} \cdot \mathbf{S}(\mathbf{q}) = 0. \tag{21}$$

These considerations lay the basis for the hyperbolic thermodynamically compatible (HTC) finite volume scheme described in the subsequent section.

3 Thermodynamically compatible finite volume scheme

In the following we assume that the two-dimensional computational domain $\Omega \subset \mathbb{R}^2$ is paved by a set of orthogonal control volumes Ω^ℓ. The common edge between two neighboring control volumes Ω^ℓ and $\Omega^\imath$ is denoted by $\partial\Omega^{\ell\imath}$, $\mathcal{n}_\ell$ is the set of neighbors of Ω^ℓ and the associated unit normal vector pointing from element Ω^ℓ to $\Omega^\imath$ is $\mathbf{n}^{\ell\imath}$, hence $\mathbf{n}^{\imath\ell} = -\mathbf{n}^{\ell\imath}$. A semi-discrete finite volume discretization in multiple space dimensions for the general form of the governing PDE system (17) with extra conservation law (18) reads

$$\begin{aligned}\frac{\partial \mathbf{q}^\ell}{\partial t} = &- \sum_{\imath \in \mathcal{n}_\ell} \frac{\left|\partial\Omega^{\ell\imath}\right|}{|\Omega^\ell|} \left(\mathcal{F}^{\ell\imath} \cdot \mathbf{n}^{\ell\imath} + \mathcal{D}\left(\mathbf{q}^\ell, \mathbf{q}^\imath\right) \cdot \mathbf{n}^{\ell\imath}\right) \\ &+ \sum_{\imath \in \mathcal{n}_\ell} \frac{\left|\partial\Omega^{\ell\imath}\right|}{|\Omega^\ell|} \left(\mathcal{G}\left(\mathbf{q}^\ell, \mathbf{q}^\imath\right) \cdot \mathbf{n}^{\ell\imath} + \mathbf{P}\left(\mathbf{q}^\ell, \mathbf{q}^\imath\right)\right) + \mathbf{S}(\mathbf{q}^\ell).\end{aligned} \tag{22}$$

The numerical flux $\mathcal{F}^{\ell\imath}\cdot\mathbf{n}^{\ell\imath}$, the fluctuations $\mathcal{D}\left(\mathbf{q}^{\ell},\mathbf{q}^{\imath}\right)\cdot\mathbf{n}^{\ell\imath}$, the dissipative terms $\mathcal{G}\left(\mathbf{q}^{\ell},\mathbf{q}^{\imath}\right)\cdot\mathbf{n}^{\ell\imath}$ with the related entropy production terms $\mathbf{P}\left(\mathbf{q}^{\ell},\mathbf{q}^{\imath}\right)$ and the algebraic source $\mathbf{S}(\mathbf{q}^{\ell})$ must verify the compatibility conditions

$$\begin{aligned}\mathbf{p}^{\ell}\cdot\left(\mathcal{F}^{\ell\imath}\cdot\mathbf{n}^{\ell\imath}-\mathbf{f}_k^{\ell}\,n_k^{\ell\imath}\right)+\mathbf{p}^{\imath}\cdot\left(\mathbf{f}_k^{\imath}\,n_k^{\ell\imath}-\mathcal{F}^{\ell\imath}\cdot\mathbf{n}^{\ell\imath}\right)\\ +\mathbf{p}^{\ell}\cdot\mathcal{D}\left(\mathbf{q}^{\ell},\mathbf{q}^{\imath}\right)\cdot\mathbf{n}^{\ell\imath}+\mathbf{p}^{\imath}\cdot\mathcal{D}\left(\mathbf{q}^{\imath},\mathbf{q}^{\ell}\right)\cdot\mathbf{n}^{\imath\ell}=\left(F_k^{\imath}-F_k^{\ell}\right)n_k^{\ell\imath},\end{aligned}\tag{23}$$

$$\mathbf{p}^{\ell}\cdot\mathbf{S}\left(\mathbf{q}^{\ell}\right)=0.\tag{24}$$

One furthermore has the usual condition $\mathcal{F}^{\imath\ell}\cdot\mathbf{n}^{\imath\ell}=-\mathcal{F}^{\ell\imath}\cdot\mathbf{n}^{\ell\imath}$ on the numerical flux. The compatibility condition on the source term (24) is automatically satisfied pointwise since the source term in PDE (17) must satisfy $\mathbf{p}\cdot\mathbf{S}=0$ due to (21). Imposing the remaining condition (23) the resulting *thermodynamically compatible* **Abgrall flux** [2,3,18] reads

$$\mathcal{F}^{\ell\imath}\cdot\mathbf{n}^{\ell\imath}=\mathcal{F}^{\ell\imath}\left(\mathbf{q}^{\ell},\mathbf{q}^{\imath}\right)\cdot\mathbf{n}^{\ell\imath}=\tilde{\mathcal{F}}^{\ell\imath}\cdot\mathbf{n}^{\ell\imath}-\alpha^{\ell\imath}\cdot\mathbf{n}^{\ell\imath}\left(\mathbf{p}^{\imath}-\mathbf{p}^{\ell}\right),\tag{25}$$

where we have used simple central approximations for the flux

$$\tilde{\mathcal{F}}^{\ell\imath}\cdot\mathbf{n}^{\ell\imath}=\tilde{\mathcal{F}}^{\ell\imath}\left(\mathbf{q}^{\ell},\mathbf{q}^{\imath}\right)\cdot\mathbf{n}^{\ell\imath}=\frac{1}{2}\left(\mathbf{f}_k^{\ell}+\mathbf{f}_k^{\imath}\right)n_k^{\ell\imath}\tag{26}$$

and for the nonconservative product

$$\mathcal{D}\left(\mathbf{q}^{\ell},\mathbf{q}^{\imath}\right)\cdot\mathbf{n}^{\ell\imath}=\frac{1}{2}\mathbf{B}_k(\bar{\mathbf{q}})n_k^{\ell\imath}\left(\mathbf{q}^{\imath}-\mathbf{q}^{\ell}\right),\quad\bar{\mathbf{q}}=\frac{1}{2}\left(\mathbf{q}^{\imath}+\mathbf{q}^{\ell}\right).\tag{27}$$

The scalar correction factor $\alpha^{\ell\imath}$ in the Abgrall flux (25), which allows to satisfy the discrete compatibility condition (23) *by construction*, is then simply obtained by inserting (25) in (23). It reads

$$\begin{aligned}\alpha^{\ell\imath}=&\frac{\left(F_k^{\imath}-F_k^{\ell}\right)n_k^{\ell\imath}+\left(\tilde{\mathcal{F}}^{\ell\imath}\cdot\mathbf{n}^{\ell\imath}\right)\cdot\left(\mathbf{p}^{\imath}-\mathbf{p}^{\ell}\right)-\left(\mathbf{p}^{\imath}\cdot\mathbf{f}_k^{\imath}-\mathbf{p}^{\ell}\cdot\mathbf{f}_k^{\ell}\right)n_k^{\ell\imath}}{\left(\mathbf{p}^{\imath}-\mathbf{p}^{\ell}\right)^2}\\&-\frac{\left(\mathbf{p}^{\imath}+\mathbf{p}^{\ell}\right)\cdot\mathcal{D}\left(\mathbf{q}^{\ell},\mathbf{q}^{\imath}\right)\cdot\mathbf{n}^{\ell\imath}}{\left(\mathbf{p}^{\imath}-\mathbf{p}^{\ell}\right)^2}.\end{aligned}\tag{28}$$

A thermodynamically compatible numerical viscosity is given by

$$\mathcal{G}\left(\mathbf{q}^{\ell},\mathbf{q}^{\imath}\right)=\epsilon^{\ell\imath}\frac{\mathbf{q}^{\imath}-\mathbf{q}^{\ell}}{\delta^{\ell\imath}}=\epsilon^{\ell\imath}\frac{\Delta\mathbf{q}^{\ell\imath}}{\delta^{\ell\imath}},\quad\delta^{\ell\imath}=\left\|\mathbf{x}^{\imath}-\mathbf{x}^{\ell}\right\|,\tag{29}$$

see [20,21,19,3,18]. The related entropy production terms read

$$\mathbf{P}\left(\mathbf{q}^{\ell},\mathbf{q}^{\imath}\right)=\left(0,0,0,\mathbf{0},\mathbf{0},\mathbf{0},\mathbf{0},\Pi_1^{\ell\imath},\Pi_2^{\ell\imath}\right)^T,\tag{30}$$

with the only non-vanishing contributions in the two entropy balance laws

$$\Pi_k^{\ell\imath}=\frac{1}{2}\epsilon^{\ell\imath}\frac{c^{k,\ell}}{T^{k,\ell}}\Delta\mathbf{q}^{\ell\imath}\,\partial^2_{\mathbf{qq}}\tilde{\mathcal{E}}^{\ell\imath}\frac{\Delta\mathbf{q}^{\ell\imath}}{\delta^{\ell\imath}},\tag{31}$$

with $k \in \{1,2\}$ and the phase temperatures T_k^ℓ computed from the equation of state of each phase. We furthermore need to define the Roe matrix of the Hessian of the energy potential, which allows us to write the numerical dissipation as usual in terms of jumps in the $\mathbf{q}$ variables rather than in terms of the main field variables $\mathbf{p}$. The Roe matrix appears in the production term (31) and reads

$$\partial^2_{\mathbf{qq}} \tilde{\mathcal{E}}^{\ell\imath} = \int_0^1 \partial^2_{\mathbf{qq}} \mathcal{E}\left(\tilde{\boldsymbol{\psi}}(s)\right) ds =: \left(\partial^2_{\mathbf{pp}} \tilde{L}^{\ell\imath}\right)^{-1}. \tag{32}$$

Inspired by the path-conservative schemes [58,24] and following previous work on HTC schemes [20,21,19,3,18] we employ a simple straight line segment path in the $\mathbf{q}$ variables in order to compute the path integral, i.e. we use

$$\tilde{\boldsymbol{\psi}}(s) = \mathbf{q}^\ell + s\left(\mathbf{q}^\imath - \mathbf{q}^\ell\right), \qquad 0 \le s \le 1. \tag{33}$$

The Roe matrix $\partial^2_{\mathbf{qq}} \tilde{\mathcal{E}}^{\ell\imath}$ computed in this manner satisfies the Roe property

$$\partial^2_{\mathbf{qq}} \tilde{\mathcal{E}}^{\ell\imath} \cdot \left(\mathbf{q}^\imath - \mathbf{q}^\ell\right) = \left(\mathbf{p}^\imath - \mathbf{p}^\ell\right) \tag{34}$$

by construction, allowing thus to rewrite jumps in the state variables $\mathbf{q}$ in terms of jumps in the dual Godunov variables (main field) $\mathbf{p}$. As in [20,21,19,3,18] the path integral appearing in (32) is approximated numerically via classical Gauss-Legendre quadrature. In practical calculation we use three quadrature points, but for the theoretical analysis of the scheme presented later we always assume that the quadrature is *exact*. The discrete algebraic source terms present in the SHTC model of compressible two-fluid flow simply reads $\mathbf{S}\left(\mathbf{q}^\ell\right)$, i.e. it corresponds to a pointwise evaluation of the source at the state $\mathbf{q}^\ell$ in cell Ω^ℓ.

Theorem 1 (Cell entropy inequalities) *The HTC FV scheme* (22) *satisfies the following two cell entropy inequalities for both phases:*

$$\frac{\partial \left(\alpha\rho s^k\right)^\ell}{\partial t} + \sum_{\imath \in n_\ell} \frac{\left|\Omega^{\ell\imath}\right|}{\left|\Omega^\ell\right|} \left(\mathcal{F}_{(\alpha\rho s^k)}\left(\mathbf{q}^\ell, \mathbf{q}^\imath\right) \cdot \mathbf{n}^{\ell\imath} - \mathcal{G}_{(\alpha\rho s^k)}\left(\mathbf{q}^\ell, \mathbf{q}^\imath\right) \cdot \mathbf{n}^{\ell\imath}\right) \ge 0, \tag{35}$$

with $k \in \{1,2\}$.

Proof The two discrete entropy evolution equations from (22) contain only conservative fluxes. Using (25), (26), (27) and (28) leads to

$$\begin{aligned} &\frac{\partial \left(\alpha\rho s^k\right)^\ell}{\partial t} + \frac{1}{\left|\Omega^\ell\right|} \sum_{\imath \in n_\ell} \left|\partial\Omega^{\ell\imath}\right| \left(\mathcal{F}_{(\alpha\rho s^k)}\left(\mathbf{q}^\ell, \mathbf{q}^\imath\right) \cdot \mathbf{n}^{\ell\imath} - \mathcal{G}_{(\alpha\rho s^k)}\left(\mathbf{q}^\ell, \mathbf{q}^\imath\right) \cdot \mathbf{n}^{\ell\imath}\right) \\ &\quad = \frac{1}{\left|\Omega^\ell\right|} \sum_{\imath \in n_\ell} \left|\partial\Omega^{\ell\imath}\right| \frac{1}{2} \epsilon^{\ell\imath} \frac{c^{k,\ell}}{T^{k,\ell}} \Delta\mathbf{q}^{\ell\imath} \cdot \partial^2_{\mathbf{qq}} \tilde{\mathcal{E}}^{\ell\imath} \frac{\Delta\mathbf{q}^{\ell\imath}}{\delta^{\ell\imath}} + \pi_k^\ell \ge 0, \end{aligned}$$

where the positivity of the right hand side is obtained thanks to $\pi_k^\ell \geq 0$ and $\Pi_k^{\ell\imath} \geq 0$ due to $c^k \geq 0$, $T^k > 0$ and the assumed positive semi-definiteness of the Hessian $\partial^2_{\mathbf{qq}}\mathcal{E}$.

Theorem 2 (Nonlinear stability in the energy norm) *The finite volume method* (22) *based on the Abgrall flux* (25) *in combination with* (26), (27), (28) *and with the source terms, the viscous flux and the discrete entropy production terms defined in* (29) *and* (31) *is nonlinearly stable in the energy norm in the sense that, for vanishing boundary fluxes, one has*

$$\int_\Omega \frac{\partial \mathcal{E}}{\partial t} d\mathbf{x} = 0. \tag{36}$$

Proof First, a semi-discrete total energy conservation law is derived by taking the dot product of the discrete Godunov variables $\mathbf{p}^\ell$ with the finite volume scheme (22):

$$\mathbf{p}^\ell \cdot \frac{\partial \mathbf{q}^\ell}{\partial t} = -\frac{1}{|\Omega^\ell|} \sum_{\imath \in n_\ell} \left|\partial\Omega^{\ell\imath}\right| \left(\mathbf{p}^\ell \cdot \left(\mathcal{F}^{\ell\imath} \cdot \mathbf{n}^{\ell\imath}\right) + \mathbf{p}^\ell \cdot \left(\mathcal{D}\left(\mathbf{q}^\ell, \mathbf{q}^\imath\right) \cdot \mathbf{n}^{\ell\imath}\right)\right)$$
$$+\frac{1}{|\Omega^\ell|} \sum_{\imath \in n_\ell} \left|\partial\Omega^{\ell\imath}\right| \left(\mathbf{p}^\ell \cdot \left(\mathcal{G}\left(\mathbf{q}^\ell, \mathbf{q}^\imath\right) \cdot \mathbf{n}^{\ell\imath}\right) + \mathbf{p}^\ell \cdot \mathbf{P}\left(\mathbf{q}^\ell, \mathbf{q}^\imath\right)\right) + \mathbf{p}^\ell \cdot \mathbf{S}(\mathbf{q}^\ell).$$

The contribution of the algebraic source terms $\mathbf{p}^\ell \cdot \mathbf{S}(\mathbf{q}^\ell)$ immediately cancels due to (24). Adding and subtracting $\frac{1}{2}\mathbf{p}^\imath \cdot \mathcal{D}\left(\mathbf{q}^\imath, \mathbf{q}^\ell\right) \cdot \mathbf{n}^{\imath\ell}$, $\frac{1}{2}\mathbf{p}^\imath \cdot \mathcal{F}^{\ell\imath} \cdot \mathbf{n}^{\ell\imath}$ and $\frac{1}{2}\mathbf{p}^\imath \cdot \mathcal{G}\left(\mathbf{q}^\ell, \mathbf{q}^\imath\right) \cdot \mathbf{n}^{\ell\imath}$ leads to

$$\begin{aligned}
\frac{\partial \mathcal{E}^\ell}{\partial t} = & -\frac{1}{|\Omega^\ell|} \sum_{\imath \in n_\ell} \left|\partial\Omega^{\ell\imath}\right| \left(\frac{1}{2}\left(\mathbf{p}^\ell + \mathbf{p}^\imath\right) \cdot \mathcal{F}^{\ell\imath} \cdot \mathbf{n}^{\ell\imath}\right) \\
& -\frac{1}{|\Omega^\ell|} \sum_{\imath \in n_\ell} \left|\partial\Omega^{\ell\imath}\right| \left(\frac{1}{2}\left(\mathbf{p}^\ell - \mathbf{p}^\imath\right) \cdot \mathcal{F}^{\ell\imath} \cdot \mathbf{n}^{\ell\imath}\right) \\
& -\frac{1}{|\Omega^\ell|} \sum_{\imath \in n_\ell} \left|\partial\Omega^{\ell\imath}\right| \left(\frac{1}{2}\mathbf{p}^\ell \cdot \mathcal{D}\left(\mathbf{q}^\ell, \mathbf{q}^\imath\right) \cdot \mathbf{n}^{\ell\imath} + \frac{1}{2}\mathbf{p}^\imath \cdot \mathcal{D}\left(\mathbf{q}^\imath, \mathbf{q}^\ell\right) \cdot \mathbf{n}^{\imath\ell}\right) \\
& -\frac{1}{|\Omega^\ell|} \sum_{\imath \in n_\ell} \left|\partial\Omega^{\ell\imath}\right| \left(\frac{1}{2}\mathbf{p}^\ell \cdot \mathcal{D}\left(\mathbf{q}^\ell, \mathbf{q}^\imath\right) \cdot \mathbf{n}^{\ell\imath} - \frac{1}{2}\mathbf{p}^\imath \cdot \mathcal{D}\left(\mathbf{q}^\imath, \mathbf{q}^\ell\right) \cdot \mathbf{n}^{\imath\ell}\right) \\
& +\frac{1}{|\Omega^\ell|} \sum_{\imath \in n_\ell} \left|\partial\Omega^{\ell\imath}\right| \left(\frac{1}{2}\left(\mathbf{p}^\ell + \mathbf{p}^\imath\right) \cdot \mathcal{G}\left(\mathbf{q}^\ell, \mathbf{q}^\imath\right) \cdot \mathbf{n}^{\ell\imath}\right) \\
& +\frac{1}{|\Omega^\ell|} \sum_{\imath \in n_\ell} \left|\partial\Omega^{\ell\imath}\right| \left(\frac{1}{2}\left(\mathbf{p}^\ell - \mathbf{p}^\imath\right) \cdot \mathcal{G}\left(\mathbf{q}^\ell, \mathbf{q}^\imath\right) \cdot \mathbf{n}^{\ell\imath} + \mathbf{p}^\ell \cdot \mathbf{P}\left(\mathbf{q}^\ell, \mathbf{q}^\imath\right)\right).
\end{aligned}$$

Using $\mathbf{n}^{\imath\ell} = -\mathbf{n}^{\ell\imath}$ together with the compatibility condition (23) yields

$$\frac{\partial \mathcal{E}^\ell}{\partial t} = -\frac{1}{|\Omega^\ell|} \sum_{\imath \in n_\ell} \left|\partial\Omega^{\ell\imath}\right| \frac{1}{2}\left(F_k^\imath - F_k^\ell\right) n_k^{\ell\imath}$$

$$
\begin{aligned}
&-\frac{1}{2\left|\Omega^{\ell}\right|}\sum_{\iota\in n_\ell}\left|\partial\Omega^{\ell\iota}\right|\left(\mathbf{p}^{\ell}\cdot\mathbf{f}_k^{\ell}-\mathbf{p}^{\iota}\cdot\mathbf{f}_k^{\iota}\right)n_k^{\ell\iota}\\
&-\frac{1}{2\left|\Omega^{\ell}\right|}\sum_{\iota\in n_\ell}\left|\partial\Omega^{\ell\iota}\right|\left(\mathbf{p}^{\ell}+\mathbf{p}^{\iota}\right)\cdot\mathcal{F}^{\ell\iota}\cdot\mathbf{n}^{\ell\iota}\\
&-\frac{1}{2\left|\Omega^{\ell}\right|}\sum_{\iota\in n_\ell}\left|\partial\Omega^{\ell\iota}\right|\left(\mathbf{p}^{\ell}\cdot\mathcal{D}\left(\mathbf{q}^{\ell},\mathbf{q}^{\iota}\right)+\mathbf{p}^{\iota}\cdot\mathcal{D}\left(\mathbf{q}^{\iota},\mathbf{q}^{\ell}\right)\right)\cdot\mathbf{n}^{\ell\iota}\\
&+\frac{1}{\left|\Omega^{\ell}\right|}\sum_{\iota\in n_\ell}\left|\partial\Omega^{\ell\iota}\right|\left(\frac{1}{2}\left(\mathbf{p}^{\ell}+\mathbf{p}^{\iota}\right)\cdot\mathcal{G}\left(\mathbf{q}^{\ell},\mathbf{q}^{\iota}\right)\cdot\mathbf{n}^{\ell\iota}\right)\\
&+\frac{1}{\left|\Omega^{\ell}\right|}\sum_{\iota\in n_\ell}\left|\partial\Omega^{\ell\iota}\right|\left(\frac{1}{2}\left(\mathbf{p}^{\ell}-\mathbf{p}^{\iota}\right)\cdot\mathcal{G}\left(\mathbf{q}^{\ell},\mathbf{q}^{\iota}\right)\cdot\mathbf{n}^{\ell\iota}+\mathbf{p}^{\ell}\cdot\mathbf{P}\left(\mathbf{q}^{\ell},\mathbf{q}^{\iota}\right)\right).
\end{aligned}
$$

Furthermore, the following identity holds

$$
\sum_{\iota\in n_\ell}\left|\partial\Omega^{\ell\iota}\right|\mathbf{n}^{\ell\iota}=0, \tag{37}
$$

since the integral of the normal vector over a closed surface vanishes. Adding $\mathbf{p}^{\ell}\cdot\mathbf{f}_k^{\ell}+F_k^{\ell}$ multiplied by (37) and using (29) and (31), we get

$$
\begin{aligned}
\frac{\partial\mathfrak{E}^{\ell}}{\partial t}=\;&-\frac{1}{\left|\Omega^{\ell}\right|}\sum_{\iota\in n_\ell}\left|\partial\Omega^{\ell\iota}\right|\frac{1}{2}\left(F_k^{\iota}+F_k^{\ell}\right)n_k^{\ell\iota}\\
&+\frac{1}{2\left|\Omega^{\ell}\right|}\sum_{\iota\in n_\ell}\left|\partial\Omega^{\ell\iota}\right|\left(\mathbf{p}^{\iota}\cdot\mathbf{f}_k^{\iota}+\mathbf{p}^{\ell}\cdot\mathbf{f}_k^{\ell}\right)n_k^{\ell\iota}\\
&-\frac{1}{2\left|\Omega^{\ell}\right|}\sum_{\iota\in n_\ell}\left|\partial\Omega^{\ell\iota}\right|\left(\mathbf{p}^{\ell}+\mathbf{p}^{\iota}\right)\cdot\mathcal{F}^{\ell\iota}\cdot\mathbf{n}^{\ell\iota}\\
&-\frac{1}{2\left|\Omega^{\ell}\right|}\sum_{\iota\in n_\ell}\left|\partial\Omega^{\ell\iota}\right|\left(\mathbf{p}^{\ell}\cdot\mathcal{D}\left(\mathbf{q}^{\ell},\mathbf{q}^{\iota}\right)+\mathbf{p}^{\iota}\cdot\mathcal{D}\left(\mathbf{q}^{\iota},\mathbf{q}^{\ell}\right)\right)\cdot\mathbf{n}^{\ell\iota}\\
&+\frac{1}{\left|\Omega^{\ell}\right|}\sum_{\iota\in n_\ell}\left|\partial\Omega^{\ell\iota}\right|\left(\frac{1}{2}\left(\mathbf{p}^{\ell}+\mathbf{p}^{\iota}\right)\cdot\mathcal{G}\left(\mathbf{q}^{\ell},\mathbf{q}^{\iota}\right)\cdot\mathbf{n}^{\ell\iota}\right)\\
&+\frac{1}{\left|\Omega^{\ell}\right|}\sum_{\iota\in n_\ell}\left|\partial\Omega^{\ell\iota}\right|\left(\frac{1}{2}\left(\mathbf{p}^{\ell}-\mathbf{p}^{\iota}\right)\cdot\epsilon^{\ell\iota}\frac{\Delta\mathbf{q}^{\ell\iota}}{\delta^{\ell\iota}}+\frac{1}{2}\epsilon^{\ell\iota}\Delta\mathbf{q}^{\ell\iota}\cdot\partial^2_{\mathbf{qq}}\tilde{\mathcal{E}}^{\ell\iota}\frac{\Delta\mathbf{q}^{\ell\iota}}{\delta^{\ell\iota}}\right).
\end{aligned}
$$

Thanks to the Roe property (34) the last two terms cancel. This leads finally to the following semi-discrete total energy conservation law with numerical total energy flux in normal direction $F_k^{\ell\iota}n_k^{\ell\iota}$:

$$
\begin{aligned}
\frac{\partial\mathfrak{E}^{\ell}}{\partial t}=\;&-\frac{1}{\left|\Omega^{\ell}\right|}\sum_{\iota\in n_\ell}\left|\partial\Omega^{\ell\iota}\right|F_k^{\ell\iota}n_k^{\ell\iota}=-\frac{1}{\left|\Omega^{\ell}\right|}\sum_{\iota\in n_\ell}\left|\partial\Omega^{\ell\iota}\right|\frac{1}{2}\left(F_k^{\iota}+F_k^{\ell}\right)n_k^{\ell\iota}\\
&-\frac{1}{\left|\Omega^{\ell}\right|}\sum_{\iota\in n_\ell}\left|\partial\Omega^{\ell\iota}\right|\frac{1}{2}\left(\mathbf{p}^{\iota}\cdot(\mathcal{F}^{\ell\iota}\cdot\mathbf{n}^{\ell\iota}-\mathbf{f}_k^{\iota}\,n_k^{\ell\iota})+\mathbf{p}^{\ell}\cdot(\mathcal{F}^{\ell\iota}\cdot\mathbf{n}^{\ell\iota}-\mathbf{f}_k^{\ell}\,n_k^{\ell\iota})\right)
\end{aligned}
$$

$$+\frac{1}{|\Omega^\ell|}\sum_{\iota\in\mathcal{N}_\ell}\left|\partial\Omega^{\ell\iota}\right|\frac{1}{2}\left(\mathbf{p}^\ell+\mathbf{p}^\iota\right)\cdot\left(\mathcal{G}\left(\mathbf{q}^\ell,\mathbf{q}^\iota\right)\cdot\mathbf{n}^{\ell\iota}\right)$$
$$-\frac{1}{2\,|\Omega^\ell|}\sum_{\iota\in\mathcal{N}_\ell}\left|\partial\Omega^{\ell\iota}\right|\left(\mathbf{p}^\ell\cdot\mathcal{D}\left(\mathbf{q}^\ell,\mathbf{q}^\iota\right)+\mathbf{p}^\iota\cdot\mathcal{D}\left(\mathbf{q}^\iota,\mathbf{q}^\ell\right)\right)\cdot\mathbf{n}^{\ell\iota}. \tag{38}$$

Summing up (38) over all elements and assuming that all fluxes and fluctuations vanish at the domain boundary and since the sum of the numerical total energy fluxes $F_k^{\ell\iota}n_k^{\ell\iota}$ at the internal interfaces cancels we obtain the sought nonlinear stability in the energy norm as

$$\int_\Omega\frac{\partial\mathcal{E}}{\partial t}d\mathbf{x}=\sum_\ell\left|\Omega^\ell\right|\frac{\partial\mathcal{E}^\ell}{\partial t}=0.$$

4 High order ADER discontinuous Galerkin finite element scheme with a posteriori subcell finite volume limiter

In order to compare and validate the results obtained with the HTC scheme introduced in the previous section, we now briefly recall the high order ADER discontinuous Galerkin (DG) finite element scheme with *a posteriori* subcell finite volume limiter [43], that was already successfully used in [20] to simulate thermodynamically compatible hyperbolic systems. Here, we will apply it to the parabolic vanishing viscosity regularization with two entropy inequalities, as well as to the asymptotically reduced Baer-Nunziato limit system, which can both be written in the general formulation of the PDE system (17).

4.1 Unlimited ADER DG schemes

As in the previous section we assume that the two-dimensional domain $\Omega\in\mathbb{R}^2$ is partitioned via a rectangular grid with elements

$$\Omega_I=\left[x_i-\frac{\Delta x}{2},x_i+\frac{\Delta x}{2}\right]\times\left[y_j-\frac{\Delta y}{2},y_j+\frac{\Delta y}{2}\right], \tag{39}$$

whose barycenters are given by $\mathbf{x}_I=(x_i,y_j)$ and the grid sizes are Δx and Δy in x- and y-direction, respectively. We seek the numerical solution $\mathbf{u}_h(\mathbf{x},t^n)$ at time n in the space of piecewise polynomials of degree N, which for each element Ω_I can be expanded in terms of basis functions $\varphi_l(\mathbf{x})$ that are tensor products of one-dimensional basis functions $\varphi_{l_m}(\chi)$ on the unit reference element $\Omega_{\text{ref}}=[0,1]$. The mapping from a position inside the reference element $\xi,\eta\in\Omega_{\text{ref}}$ onto the cell Ω_I is given by $x=x_i-\frac{1}{2}\Delta x+\xi\Delta x$ and $y=y_j-\frac{1}{2}\Delta y+\eta\Delta y$. The basis functions on the reference element are defined as the Lagrange interpolation polynomials passing through the Gauss-Legendre quadrature nodes of a Gaussian quadrature formula with $N+1$ quadrature

nodes. This leads to an orthogonal nodal basis by construction and we finally obtain

$$\mathbf{u}_h(\mathbf{x}, t^n) = \varphi_l(\mathbf{x})\hat{\mathbf{u}}^n_{l,I}, \quad \mathbf{x} \in \Omega_I, \tag{40}$$

where the coefficients $\hat{\mathbf{u}}^n_{l,I}$ are constant within Ω_I. Multiplying the PDE system (17) by a test function φ_l and integrating over the space time control volume $\Omega_I \times [t^n, t^{n+1}]$ leads to

$$\begin{aligned}
&\int_{t^n}^{t^{n+1}} \int_{\Omega_I} \varphi_l \left(\partial_t \mathbf{q} + \nabla \cdot \mathbf{f}(\mathbf{q}) + \mathbf{B}(\mathbf{q}) \cdot \nabla \mathbf{q} - \nabla \cdot (\epsilon \nabla \mathbf{q})\right) d\mathbf{x}\, dt \\
&= \int_{t^n}^{t^{n+1}} \int_{\Omega_I} \varphi_l \left(\mathbf{P}(\mathbf{q}, \nabla \mathbf{q}) + \mathbf{S}(\mathbf{q})\right) d\mathbf{x}\, dt.
\end{aligned}$$

Note that according to the Galerkin approach, the test functions are chosen identical to the basis functions. Replacing $\mathbf{q}$ in the first term by the numerical solution $\mathbf{u}_h$ as given in (40) and by the element-local space-time predictor $\mathbf{q}_h$ described later in all remaining terms, we obtain via integration by parts

$$\begin{aligned}
&(\varphi_l \varphi_k) \left(\hat{\mathbf{u}}^{n+1}_{k,I} - \hat{\mathbf{u}}^n_{k,I}\right) + \int_{t^n}^{t^{n+1}} \int_{\partial\Omega_I} \varphi_l \left(\mathcal{F}\left(\mathbf{q}_h^-, \mathbf{q}_h^+\right) + \mathcal{D}\left(\mathbf{q}_h^-, \mathbf{q}_h^+\right)\right) \cdot \mathbf{n}\, dS\, dt \\
&- \int_{t^n}^{t^{n+1}} \int_{\partial\Omega_I} \varphi_l \mathcal{G}\left(\mathbf{q}_h^-, \mathbf{q}_h^+\right) \cdot \mathbf{n}\, dS\, dt \\
&- \int_{t^n}^{t^{n+1}} \int_{\Omega_I} \nabla \varphi_l \cdot \mathbf{f}(\mathbf{q}_h)\, d\mathbf{x}\, dt + \int_{t^n}^{t^{n+1}} \int_{\Omega_I^\circ} \varphi_l \mathbf{B}(\mathbf{q}_h) \cdot \nabla \mathbf{q}_h\, d\mathbf{x}\, dt \\
&+ \int_{t^n}^{t^{n+1}} \int_{\Omega_I} \nabla \varphi_l \cdot \epsilon \nabla \mathbf{q}_h\, d\mathbf{x}\, dt \\
&= \int_{t^n}^{t^{n+1}} \int_{\Omega_I} \varphi_l \left(\mathbf{P}(\mathbf{q}_h, \nabla \mathbf{q}_h) + \mathbf{S}(\mathbf{q}_h)\right) d\mathbf{x}\, dt,
\end{aligned} \tag{41}$$

where $\mathbf{n}$ denotes the outward-pointing unit normal vector at the cell boundary $\partial\Omega_I$. For the numerical flux in normal direction $\mathcal{F} \cdot \mathbf{n}$ at the cell interfaces we use the Rusanov flux as approximate Riemann solver,

$$\mathcal{F}\left(\mathbf{q}_h^-, \mathbf{q}_h^+\right) \cdot \mathbf{n} = \frac{1}{2}\left(\mathbf{f}(\mathbf{q}_h^+) + \mathbf{f}(\mathbf{q}_h^-)\right) \cdot \mathbf{n} - \frac{1}{2} s_{\max}\, \mathbb{I}\, (\mathbf{q}_h^+ - \mathbf{q}_h^-), \tag{42}$$

with the maximum signal speed at the interface $s_{\max} = \max\left(|\lambda_l(\mathbf{q}_h^-)|, |\lambda_l(\mathbf{q}_h^+)|\right)$ and $\mathbb{I}$ the identity matrix. For further choices see e.g. [74]. For the dissipative terms we set

$$\mathcal{G}\left(\mathbf{q}_h^-, \mathbf{q}_h^+\right) \cdot \mathbf{n} = \epsilon\, \frac{2N+1}{\Delta x}\, \mathbb{I}\, \left(\mathbf{q}_h^+ - \mathbf{q}_h^-\right), \tag{43}$$

see also [46], and for the non-conservative product, a path conservative method as forwarded by Castro, Parés and collaborators [23,24,55,58], which is based

on the theoretical background outlined by Dal Maso, Le Floch and Murat in [54]. We employ a simple linear segment path

$$\Psi(s,\mathbf{q}_h^-,\mathbf{q}_h^+) = \mathbf{q}_h^- + s(\mathbf{q}_h^+ - \mathbf{q}_h^-) \quad \text{for} \quad s\in[0,1], \tag{44}$$

yielding

$$\mathcal{D}(\mathbf{q}_h^-,\mathbf{q}_h^+)\cdot\mathbf{n} = \frac{1}{2}\tilde{\mathbf{B}}\cdot\left(\mathbf{q}_h^+ - \mathbf{q}_h^-\right) \quad \text{with} \quad \tilde{\mathbf{B}} = \int_0^1 \mathbf{B}(\Psi(s,\mathbf{q}_h^-,\mathbf{q}_h^+))\cdot\mathbf{n}\, ds. \tag{45}$$

The arising integral for $\tilde{\mathbf{B}}$ is approximated numerically with a Gauss quadrature rule of sufficient order of accuracy.

Note that to obtain the polynomial coefficients at the new time $\hat{\mathbf{u}}_{k,I}^{n+1}$ from (41), the space-time predictor $\mathbf{q}_h$ and the boundary extrapolated values $\mathbf{q}_h^-$ and $\mathbf{q}_h^+$ between two neighboring cells Ω_I and Ω_J have to be known. Following [17,37,39,43] , the space-time predictor $\mathbf{q}_h(\mathbf{x},t)$ is obtained using the weak formulation of (17) in space-time, thus avoiding the Cauchy-Kovalewskaya procedure on which standard ADER schemes are based, see e.g. [72,73,75,22]. In a similar fashion than in the definition of $\mathbf{u}_h(\mathbf{x},t)$ we set

$$\mathbf{q}(\mathbf{x},t) = \theta_l(\mathbf{x},t)\hat{\mathbf{q}}_{l,I}^n, \quad \text{on} \quad \Omega_I\times[t^n,t^{n+1}], \tag{46}$$

where the *space-time* basis functions $\theta_l(\mathbf{x},t)$ are now tensor products of the one-dimensional basis functions φ_{l_m} and a temporal basis function, given by

$$\theta_l(\mathbf{x},t) = \varphi_{l_0}(\tau)\varphi_{l_1}(\xi)\varphi_{l_2}(\eta), \quad t = t^n + \tau\Delta t, \quad \tau,\xi,\eta\in[0,1]. \tag{47}$$

Multiplying (17) now by the space-time test function θ_l and integrating over $\Omega_I\times[t^n,t^{n+1}]$ yields

$$\begin{aligned}
&\int_{t^n}^{t^{n+1}}\int_{\Omega_I} \theta_l\left(\partial_t\mathbf{q} + \nabla\cdot\mathbf{f}(\mathbf{q}) + \mathbf{B}(\mathbf{q})\cdot\nabla\mathbf{q} - \nabla\cdot(\epsilon\nabla\mathbf{q})\right)\, d\mathbf{x}\, dt\\
&= \int_{t^n}^{t^{n+1}}\int_{\Omega_I} \theta_l\left(\mathbf{P}(\mathbf{q},\nabla\mathbf{q}) + \mathbf{S}(\mathbf{q})\right)\, d\mathbf{x}\, dt.
\end{aligned}$$

After integration by parts of the term containing the time derivative and taking into account the known initial condition of the element-local Cauchy problem given by $\mathbf{u}_h$ at time t^n, we obtain

$$\begin{aligned}
&\int_{\Omega_I}\theta_l(\mathbf{x},t^{n+1})\mathbf{q}_h(\mathbf{x},t^{n+1})\, d\mathbf{x} - \int_{\Omega_I}\theta(\mathbf{x},t^n)\mathbf{u}_h(\mathbf{x},t^n)\, d\mathbf{x}\\
&- \int_{t^n}^{t^{n+1}}\int_{\Omega_I}\left(\partial_t\theta_l\right)\mathbf{q}_h(\mathbf{x},t)\, d\mathbf{x}\, dt\\
&+ \int_{t^n}^{t^{n+1}}\int_{\Omega_I}\theta_l\left(\nabla\cdot\mathbf{f}(\mathbf{q}_h) + \mathbf{B}(\mathbf{q}_h)\cdot\nabla\mathbf{q}_h - \nabla\cdot(\epsilon\nabla\mathbf{q}_h)\right)\, d\mathbf{x}\, dt\\
&= \int_{t^n}^{t^{n+1}}\int_{\Omega_I}\theta_l\left(\mathbf{P}(\mathbf{q}_h,\nabla\mathbf{q}_h) + \mathbf{S}(\mathbf{q}_h)\right)\, d\mathbf{x}\, dt.
\end{aligned} \tag{48}$$

Using (46), equation (48) can be reformulated in a non-linear element-local algebraic system for the coefficients $\hat{\mathbf{q}}_{l,I}^n$, which is solved by an iterative solver whose convergence was proven in [17] for the case of hyperbolic conservation laws without non-conservative products. Once the space-time predictor $\mathbf{q}_h$ is determined for all elements, the polynomial coefficients $\hat{\mathbf{u}}^{n+1}$ are obtained from (41).

4.2 A posteriori subcell finite volume limiter

The unlimited ADER-DG scheme presented in the previous section is high order accurate, but linear in the sense of Godunov, which means that it will generate spurious oscillations near shock waves and discontinuities, according to the well-known Godunov theorem. To avoid exactly these non-physical artifacts, a new *a posteriori* subcell limiter was introduced in [43,76,41,15] for ADER-DG schemes based on the MOOD framework for finite volume schemes [29,35,30].

First, a so-called candidate solution $\mathbf{u}_h^*(\mathbf{x}, t^{n+1})$ is computed with the unlimited ADER-DG scheme described in the previous section. Then, *a posteriori*, the candidate solution is checked against several numerical and physical detection criteria, like the positivity of the density and the pressure and the absence of floating point errors. Furthermore, we require that a discrete maximum principle is fulfilled [43]. If any of these numerical or physical detection criteria is violated inside a DG element, it is marked as troubled cell and is scheduled for the *a posteriori* subcell FV limiting. All flagged cells Ω_I are split into $(2N+1)^2$ FV subcells Ω_I^s with $\Omega_I = \bigcup_s \Omega_I^s$. This process does not reduce the time step of the DG scheme, since the CFL number of an explicit DG scheme scales with $1/(2N+1)$, while the CFL condition of FV methods is bounded from above by one. As standard in the FV framework, the solution on the subcells Ω_I^s is approximated via piecewise constant cell averages

$$\bar{\mathbf{u}}_{I,s}^n = \frac{1}{|\Omega_I^s|} \int_{\Omega_I^s} \mathbf{u}_h(\mathbf{x}, t^n)\, d\mathbf{x} \tag{49}$$

obtained from the high order DG polynomials $\mathbf{u}_h(\mathbf{x}, t^n)$. Then the subcell averages are either evolved in time with a second order MUSCL-Hancock-type TVD FV scheme with minmod limiter or a third order ADER-WENO FV scheme, see [43]. Both schemes are predictor-corrector methods as the ADER-DG scheme itself, and can be written in the DG framework by employing a unity test function thus reducing the method to solving

$$\begin{aligned}
&|\Omega_I^s| \left(\bar{\mathbf{u}}_{I,s}^{n+1} - \bar{\mathbf{u}}_{I,s}^n \right) \\
&+ \int_{t^n}^{t^{n+1}} \int_{\partial\Omega_I^s} \left(\mathcal{F}\left(\mathbf{q}_h^-, \mathbf{q}_h^+\right) + \mathcal{D}\left(\mathbf{q}_h^-, \mathbf{q}_h^+\right) - \mathcal{G}\left(\mathbf{q}_h^-, \mathbf{q}_h^+\right) \right) \cdot \mathbf{n}\, dS\, dt \\
&+ \int_{t^n}^{t^{n+1}} \int_{\Omega_I^{s,\circ}} \mathbf{B}(\mathbf{q}_h) \cdot \nabla \mathbf{q}_h\, d\mathbf{x}\, dt
\end{aligned}$$

$$= \int_{t^n}^{t^{n+1}} \int_{\Omega_I^s} \left(\mathbf{P}(\mathbf{q}_h, \nabla \mathbf{q}_h) + \mathbf{S}(\mathbf{q}_h) \right) d\mathbf{x}\, dt. \tag{50}$$

Once the cell averages $\bar{\mathbf{u}}_{I,s}^{n+1}$ of all subcells in Ω_I are obtained, the limited DG polynomials $\mathbf{u}_h'(\mathbf{x}, t^{n+1})$ at the new time are obtained via a constrained least squares reconstruction requiring the conservation of the solution on the subcells C_I^s

$$\frac{1}{|\Omega_{I,s}|} \int_{\Omega_{I,s}} \mathbf{u}_h'(\mathbf{x}, t^{n+1})\, d\mathbf{x} = \bar{\mathbf{u}}_{I,s}^{n+1} \tag{51}$$

and the conservation of the solution within the element Ω_I

$$\int_{\Omega_I} \mathbf{u}_h'(\mathbf{x}, t^{n+1})\, d\mathbf{x} = \sum_{\forall \Omega_I^s \subset \Omega_I} |\Omega_I^s| \bar{\mathbf{u}}_{I,s}^{n+1}. \tag{52}$$

Since it is very likely that a cell is also flagged as a troubled cell also in the subsequent time step, for instance close to a discontinuity, the FV subcell averages $\bar{\mathbf{u}}_{I,s}^{n+1}$ are kept in memory, to be used as initial condition for the limiting processes in the next time step. For further details, see also [43,41, 77]. This concludes the description of the ADER-DG scheme with a posteriori subcell FV limiting.

5 Numerical results

In this section, we present several numerical test cases aiming at assessing the proposed new semi-discrete HTC scheme for the two-fluid model with two entropy inequalities. As time integrator the classical fourth order Runge-Kutta method is used for all test problems shown below. Besides, the time step is set according to the CFL-type condition

$$\Delta t = \frac{\mathrm{CFL}}{2N+1} \frac{1}{\frac{|\lambda_{\max}|}{h} + 2\,\epsilon\,\frac{2N+1}{h^2}} \tag{53}$$

with $h = \min(\Delta x, \Delta y)$ the characteristic mesh spacing, $|\lambda_{\max}|$ the maximum absolute value of the eigenvalues in the domain and $\mathrm{CFL} < d$, where d is the number of space dimensions.

5.1 Numerical convergence study

To verify the numerical convergence of the new HTC scheme and the ADER-DG in the vanishing viscosity approach, we construct a smooth solution of the full two-fluid model (3) given by a stationary vortex with zero radial velocities and and constant movement in angular direction. Therefore we consider the polar coordinate representation (65) given in Appendix A and set

$$v_r = 0, \quad w_r = 0, \quad j_r^1 = 0, \quad j_r^2 = 0, \quad \frac{\partial}{\partial t}(\cdot) = 0, \quad \frac{\partial}{\partial \theta}(\cdot) = 0. \tag{54}$$

Equations (65) reduce then to solving

$$\frac{\partial p}{\partial r} = \frac{\alpha^1\rho^1(v_\theta^1)^2 + \alpha^2\rho^2(v_\theta^2)^2}{r}, \tag{55a}$$

$$\frac{\partial}{\partial r}\left(\frac{(v_\theta^1)^2 - (v_\theta^2)^2}{2} + \mu_1 - \mu_2\right) - v_\theta\left(\frac{1}{r}\frac{\partial}{\partial r}(rw_\theta)\right) = 0 \tag{55b}$$

$$\frac{\partial T^1}{\partial r} = \frac{\rho j_\theta^1 v_\theta}{r}, \tag{55c}$$

$$\frac{\partial T^2}{\partial r} = \frac{\rho j_\theta^2 v_\theta}{r}, \tag{55d}$$

with $p = \alpha^1 p^1 + \alpha^2 p^2,\ w_\theta = v_\theta^1 - v_\theta^2,\ v_\theta = c^1 v_\theta^1 + c^2 v_\theta^2$.

We give the profiles of the phase velocities and thermal impulses as

$$v_\theta^l = r v_a^l \exp(\nu_v^l(1-r^2)), \quad j_\theta^l = r j_a^l \exp(\nu_j^l(1-r^2))$$

and the profile for the volume fraction as

$$\alpha^1 = c_\alpha + \alpha_c \exp(\nu_\alpha(1-r^2)).$$

The four unknowns ρ^l and T^l can be determined via the following system of ordinary differential equations (ODEs) based on the EOS (2)

$$\begin{pmatrix} \alpha^1\frac{\partial p^1}{\partial \rho^1} & \alpha^2\frac{\partial p^2}{\partial \rho^2} & \alpha^1\frac{\partial p^1}{\partial T^1} & \alpha^2\frac{\partial p^2}{\partial T^2} \\ \frac{\partial \mu^1}{\partial \rho^1} & -\frac{\partial \mu^2}{\partial \rho^2} & \frac{\partial \mu^1}{\partial T^1} & -\frac{\partial \mu^2}{\partial T^2} \\ 0 & 0 & 1 & 0 \\ 0 & 0 & 0 & 1 \end{pmatrix} \begin{pmatrix} \frac{\partial \rho^1}{\partial r} \\ \frac{\partial \rho^2}{\partial r} \\ \frac{\partial T^1}{\partial r} \\ \frac{\partial T^2}{\partial r} \end{pmatrix} =$$

$$\begin{pmatrix} \frac{\alpha^1\rho^1(v_\theta^1)^2 + \alpha^2\rho^2(v_\theta^2)^2}{r} - p^1\frac{\partial \alpha^1}{\partial r} + p^2\frac{\partial \alpha^1}{\partial r} \\ -\frac{\partial}{\partial r}\left(\frac{(v_\theta^1)^2 - (v_\theta^2)^2}{2}\right) + v_\theta\left(\frac{1}{r}\frac{\partial}{\partial r}(rw_\theta)\right) - A^1 j_\theta^1\frac{\partial j_\theta^1}{\partial r} + A^2 j_\theta^2\frac{\partial j_\theta^2}{\partial r} \\ \frac{\rho j_\theta^1 v_\theta}{r} \\ \frac{\rho j_\theta^2 v_\theta}{r} \end{pmatrix} \tag{56}$$

with

$$\frac{\partial p^1}{\partial \rho^1} = (\gamma^1 - 1)c_v^1 T^1, \qquad \frac{\partial p^2}{\partial \rho^2} = (\gamma^2 - 1)c_v^2 T^2 \tag{57a}$$

$$\frac{\partial p^1}{\partial T^1} = (\gamma^1 - 1)c_v^1 \rho^1, \qquad \frac{\partial p^2}{\partial T^2} = (\gamma^2 - 1)c_v^2 \rho^2 \tag{57b}$$

	32		64		128		256		512	
α^1	1.92E-03	—	4.65E-04	2.0	1.18E-04	2.0	3.02E-05	2.0	7.59E-06	2.0
ρ^1	5.01E-02	—	1.28E-02	2.0	3.22E-03	2.0	8.07E-04	2.0	2.02E-04	2.0
ρ^2	2.16E-02	—	5.37E-03	2.0	1.33E-03	2.0	3.31E-04	2.0	8.27E-05	2.0
v_1^1	1.99E-02	—	5.51E-03	1.9	1.42E-03	2.0	3.57E-04	2.0	8.94E-05	2.0
v_2^1	1.99E-02	—	5.51E-03	1.9	1.42E-03	2.0	3.57E-04	2.0	8.94E-05	2.0
v_1^2	2.59E-02	—	7.24E-03	1.8	1.87E-03	2.0	4.70E-04	2.0	1.18E-04	2.0
v_2^2	2.59E-02	—	7.24E-03	1.8	1.87E-03	2.0	4.70E-04	2.0	1.18E-04	2.0
j_1^1	2.40E-03	—	6.79E-04	1.8	1.78E-04	1.9	4.52E-05	2.0	1.13E-05	2.0
j_2^1	2.40E-03	—	6.79E-04	1.8	1.78E-04	1.9	4.52E-05	2.0	1.13E-05	2.0
j_1^2	2.05E-03	—	6.09E-04	1.7	1.66E-04	1.9	4.26E-05	2.0	1.07E-05	2.0
j_2^2	2.05E-03	—	6.09E-04	1.7	1.66E-04	1.9	4.26E-05	2.0	1.07E-05	2.0
p^1	1.41E-01	—	3.57E-02	2.0	8.95E-03	2.0	2.24E-03	2.0	5.60E-04	2.0
p^2	1.58E-01	—	3.84E-02	2.0	9.56E-03	2.0	2.39E-03	2.0	5.98E-04	2.0
ρE	2.40E-01	—	6.15E-02	2.0	1.54E-03	2.0	3.87E-03	2.0	9.69E-04	2.0

Table 1 Twofluid stationary vortex: L^2 error and EOC for the new HTC scheme.

$$\frac{\partial \mu^1}{\partial \rho^1} = \frac{(\gamma^1 - 1) c_v^1 T^1}{\rho^1}, \qquad \frac{\partial \mu^2}{\partial \rho^2} = \frac{(\gamma^2 - 1) c_v^2 T^2}{\rho^2} \tag{57c}$$

$$\frac{\partial \mu^1}{\partial T^1} = (\gamma^1 - 1) c_v^1 - s^1, \qquad \frac{\partial \mu^1}{\partial T^1} = (\gamma^2 - 1) c_v^2 - s^2. \tag{57d}$$

We set the following parameters in the initial condition

$$\begin{aligned} &\gamma^1 = 1.4, && \gamma^2 = 2, && c_v^1 = 1, && c_v^2 = 2, \\ &v_a^1 = 1, && v_a^2 = 1.5, && \nu_v^1 = 1, && \nu_v^2 = 1.2, \\ &j_a^1 = 0.1, && j_a^2 = 0.1, && \nu_j^1 = 1, && \nu_j^2 = 1.2, \\ &c_\alpha = 0.4, && \alpha_c = 0.1, && \nu_a = 0.5, && A^1 = 10, \quad A^2 = 10. \end{aligned}$$

The initial values for the ODE system (56) are given by $\rho^1 = 1.5, \rho^2 = 1, T^1 = 4, T^2 = 2$ and the vortex solution in polar coordinates is obtained numerically with RK4. The computational domain for the vortex in Cartesian coordinates is given by $[-5, 5] \times [-5, 5]$ with periodic boundary conditions and the vortex is run up to a final time $T_f = 0.1$. In Tables 1 to 5 the L^2 error at the final time and experimental order of convergence (EOC) of the new HTC scheme with two entropy inequalities and the ADER-DG scheme with $N = 2, \dots, 5$ are given. We obtain the expected EOC of 2 for the HTC and the corresponding higher order convergence for the ADER-DG scheme.

	16		32		64		128		256	
α^1	5.45E-04	—	1.03E-04	2.4	2.06E-05	2.3	3.93E-06	2.4	6.97E-07	2.5
ρ^1	3.01E-02	—	7.25E-03	2.1	1.30E-03	2.5	2.00E-04	2.7	2.93E-05	2.8
ρ^2	1.28E-02	—	2.87E-03	2.2	5.42E-04	2.4	8.56E-05	2.7	1.25E-05	2.8
v_1^1	1.46E-02	—	3.63E-03	2.0	8.21E-04	2.1	1.68E-04	2.3	3.12E-05	2.4
v_2^1	1.46E-02	—	3.63E-03	2.0	8.21E-04	2.1	1.68E-04	2.3	3.12E-05	2.4
v_1^2	2.45E-02	—	5.31E-03	2.2	1.09E-03	2.3	2.03E-04	2.4	3.57E-05	2.5
v_2^2	2.45E-02	—	5.31E-03	2.2	1.09E-03	2.3	2.03E-04	2.4	3.57E-05	2.5
j_1^1	1.85E-03	—	3.44E-04	2.4	6.76E-05	2.3	1.37E-05	2.3	2.57E-06	2.4
j_2^1	1.85E-03	—	3.44E-04	2.4	6.76E-05	2.3	1.37E-05	2.3	2.57E-06	2.4
j_1^2	1.72E-03	—	4.86E-04	1.8	1.27E-04	1.9	2.40E-05	2.4	4.43E-06	2.4
j_2^2	1.72E-03	—	4.86E-04	1.8	1.27E-04	1.9	2.40E-05	2.4	4.43E-06	2.4
p^1	6.55E-02	—	1.43E-02	2.2	2.44E-03	2.6	3.66E-04	2.7	5.37E-05	2.8
p^2	1.03E-01	—	2.50E-02	2.0	4.53E-03	2.5	7.13E-04	2.7	1.03E-04	2.8
ρE	1.49E-01	—	3.37E-02	2.1	6.14E-03	2.5	1.03E-03	2.6	1.66E-04	2.6

Table 2 Twofluid stationary vortex: L^2 error and EOC for ADER-DG with $N = 2$.

	16		24		32		48		64	
α^1	2.84E-05	—	5.56E-06	4.0	1.36E-06	4.9	1.71E-07	5.1	4.13E-08	4.9
ρ^1	5.56E-03	—	2.31E-03	2.2	4.18E-04	5.9	7.28E-05	4.3	1.66E-05	5.1
ρ^2	3.83E-03	—	5.27E-04	4.9	1.33E-04	4.8	1.69E-05	5.1	4.44E-06	4.7
v_1^1	8.73E-03	—	2.04E-03	3.6	3.95E-04	5.7	5.27E-05	5.0	1.17E-05	5.2
v_2^1	8.73E-03	—	2.04E-03	3.6	3.95E-04	5.7	5.27E-05	5.0	1.17E-05	5.2
v_1^2	7.01E-03	—	1.77E-03	3.4	3.73E-04	5.4	4.90E-05	5.0	1.11E-05	5.2
v_2^2	7.01E-03	—	1.77E-03	3.4	3.73E-04	5.4	4.90E-05	5.0	1.11E-05	5.2
j_1^1	8.31E-04	—	1.83E-04	3.7	4.63E-05	4.8	7.47E-06	4.5	1.92E-06	4.7
j_2^1	8.31E-04	—	1.83E-04	3.7	4.63E-05	4.8	7.47E-06	4.5	1.92E-06	4.7
j_1^2	7.98E-04	—	2.28E-04	3.1	4.52E-05	5.6	6.58E-06	4.7	1.41E-06	5.4
j_2^2	7.98E-04	—	2.28E-04	3.1	4.52E-05	5.6	6.58E-06	4.7	1.41E-06	5.4
p^1	1.06E-02	—	4.17E-03	2.3	8.09E-04	5.7	1.30E-04	4.5	3.18E-05	4.9
p^2	2.73E-02	—	4.00E-03	4.7	1.12E-03	4.4	1.25E-04	5.4	3.43E-05	4.5
ρE	3.08E-02	—	1.11E-02	2.5	2.21E-03	5.6	3.39E-04	4.6	8.21E-05	4.9

Table 3 Twofluid stationary vortex: L^2 error and EOC for ADER-DG with $N = 3$.

	16		24		32		48		64	
α^1	2.61E-06	—	5.85E-07	3.7	1.84E-07	4.0	3.45E-08	4.1	9.86E-09	4.4
ρ^1	6.55E-04	—	1.00E-04	4.6	4.03E-05	3.2	7.96E-06	4.0	2.43E-06	4.1
ρ^2	1.45E-04	—	4.01E-05	3.2	1.13E-05	4.4	2.16E-06	4.1	6.06E-07	4.4
v_1^1	4.25E-04	—	1.01E-04	3.5	3.28E-05	3.9	7.02E-06	3.8	2.22E-06	4.0
v_2^1	4.25E-04	—	1.01E-04	3.5	3.28E-05	3.9	7.02E-06	3.8	2.22E-06	4.0
v_1^2	4.29E-04	—	9.72E-05	3.7	2.99E-05	4.1	6.24E-06	3.9	1.97E-06	4.0
v_2^2	4.29E-04	—	9.72E-05	3.7	2.99E-05	4.1	6.24E-06	3.9	1.97E-06	4.0
j_1^1	1.09E-04	—	1.79E-05	4.4	4.19E-06	5.1	7.38E-07	4.3	2.20E-07	4.2
j_2^1	1.09E-04	—	1.79E-05	4.4	4.19E-06	5.1	7.38E-07	4.3	2.20E-07	4.2
j_1^2	5.36E-05	—	1.25E-05	3.6	3.79E-06	4.2	7.76E-07	3.9	2.42E-07	4.0
j_2^2	5.36E-05	—	1.25E-05	3.6	3.79E-06	4.2	7.76E-07	3.9	2.42E-07	4.0
p^1	1.33E-03	—	2.01E-04	4.7	7.08E-05	3.6	1.31E-05	4.2	3.91E-06	4.2
p^2	1.20E-03	—	3.08E-04	3.4	8.53E-05	4.5	1.58E-05	4.2	4.53E-06	4.3
ρE	3.00E-03	—	4.81E-04	4.5	1.85E-04	3.3	3.70E-05	4.0	1.15E-05	4.1

Table 4 Twofluid stationary vortex: L^2 error and EOC for ADER-DG with $N = 4$.

	8		16		24		32		48	
α^1	2.20E-05	—	9.14E-07	4.6	1.12E-07	5.2	1.26E-08	7.6	7.65E-10	6.9
ρ^1	9.21E-03	—	2.14E-04	5.4	4.56E-05	3.8	3.83E-06	8.6	5.10E-07	5.0
ρ^2	2.13E-03	—	1.27E-04	4.1	7.64E-06	6.9	1.92E-06	4.8	9.93E-08	7.3
v_1^1	5.77E-03	—	3.33E-04	4.1	3.82E-05	5.3	3.54E-06	8.3	3.25E-07	5.9
v_2^1	5.77E-03	—	3.33E-04	4.1	3.82E-05	5.3	3.54E-06	8.3	3.25E-07	5.9
v_1^2	6.41E-03	—	2.86E-04	4.5	3.54E-05	5.2	3.84E-06	7.7	3.40E-07	6.0
v_2^2	6.41E-03	—	2.86E-04	4.5	3.54E-05	5.2	3.84E-06	7.7	3.40E-07	6.0
j_1^1	6.75E-04	—	3.51E-05	4.3	3.96E-06	5.4	5.88E-07	6.6	4.94E-08	6.1
j_2^1	6.75E-04	—	3.51E-05	4.3	3.96E-06	5.4	5.88E-07	6.6	4.94E-08	6.1
j_1^2	7.87E-04	—	3.69E-05	4.4	4.94E-06	5.0	4.35E-07	8.4	4.72E-08	5.5
j_2^2	7.87E-04	—	3.69E-05	4.4	4.94E-06	5.0	4.35E-07	8.4	4.72E-08	5.5
p^1	1.64E-02	—	3.65E-04	5.5	7.27E-05	4.0	7.53E-06	7.9	8.18E-07	5.5
p^2	1.82E-02	—	7.94E-04	4.5	4.85E-05	6.9	1.36E-05	4.4	6.39E-07	7.5
ρE	4.45E-02	—	9.92E-04	5.5	2.02E-04	3.9	2.10E-05	7.9	2.03E-06	5.8

Table 5 Twofluid stationary vortex: L^2 error and EOC for ADER-DG with $N = 5$.

Test	T_f	state	α^1	ρ^1	ρ^2	v_1^1	v_1^2	p^1	p^2
RP1	0.3	left	0.8	1	0.2	0	0	1	0.3
		right	0.3	1	1	0	0	1	1
RP2	0.3	left	0.7	1	2	-1	-1	1	1
		right	0.3	1	2	1	1	1	1

Table 6 Initial condition for the 1D Riemann problems presented in Section 5.2 with $\gamma^1 = 1.4$ and $\gamma^2 = 2$.

5.2 1D Riemann problems

Next, we consider two Riemann Problems (RP) on the computational domain $[-1, 1]$ for the twofluid model (3) without relaxation processes (green terms), thus we set $\zeta = 0$ and formally $\tau = \infty$. Further we set as in the previous test case $\gamma^1 = 1.4$, $\gamma^2 = 2$ under the ideal gas law (2). We assume a moderate influence of the thermal impulses on the internal energy setting $A^1 = 1, A^2 = 1$, where the initial thermal impulses are set to zero $\mathbf{j}^1 = 0$, $\mathbf{j}^2 = 0$. For the remaining phase variables the initial configurations of left and right states separated by a discontinuity placed at $x = 0$ are given in Table 6. The first Riemann problem (RP1) consists of a jump in the volume fraction, phase density 2 and pressure 2 with zero initial velocity resulting in a discontinuous mixture density and pressure. The second Riemann problem (RP2) is a double rarefaction test with constant initial phase densities and pressures, whereas we have a jump in the volume fraction resulting in a discontinuous mixture density and pressure. In Figures 1, we compare the HTC FV scheme with 4096 cells against the ADER-DG scheme with $N = 3$ and 512 elements in the vanishing viscosity limit (VVL) with $\epsilon = 5 \cdot 10^{-4}$ for the mixture density, velocity, pressure and relative velocity of RP1. Since there are no heat and shear processes present, the Riemann problem consists of 9 waves in total that can be best observed in the relative velocity. We find a very good agreement between the HTC FV scheme and the ADER-DG VVL where both graphs are superimposed. The same applies to the rarefaction test case RP2 displayed in Figure 2 which consists of 4 waves traveling to the boundaries of the domain with a contact in the mixture density due to the initial jump of the volume fraction. Even though the viscosity $\epsilon = 10^{-4}$ applied in the ADER-DG scheme is still quite large, we find a very good match between the two schemes which validates the new HTC approach with two entropy inequalities to yield the correct shock speeds and amplitudes for both Riemann Problems.

Next, we verify numerically the stiff heat relaxation limit of the twofluid model (3) with the limit Baer-Nunziato-Fourier type model (12). This is done by comparing the HTC FV scheme and the ADER-DG VVL scheme applied on the two-fluid model (3) with the ADER-DG scheme applied on the Baer-Nunziato model (12) with the parabolic temperature terms in the phase energies. In order to do this comparison, we increase the influence of the thermal impulses setting $A^1 = A^2 = 400$ and the thermal conductivity coeffients $\kappa^1 = \kappa^2 = 2 \cdot 10^{-3}$ yielding a heat relaxation rate $\tau = \mathcal{O}(10^{-6})$. The results

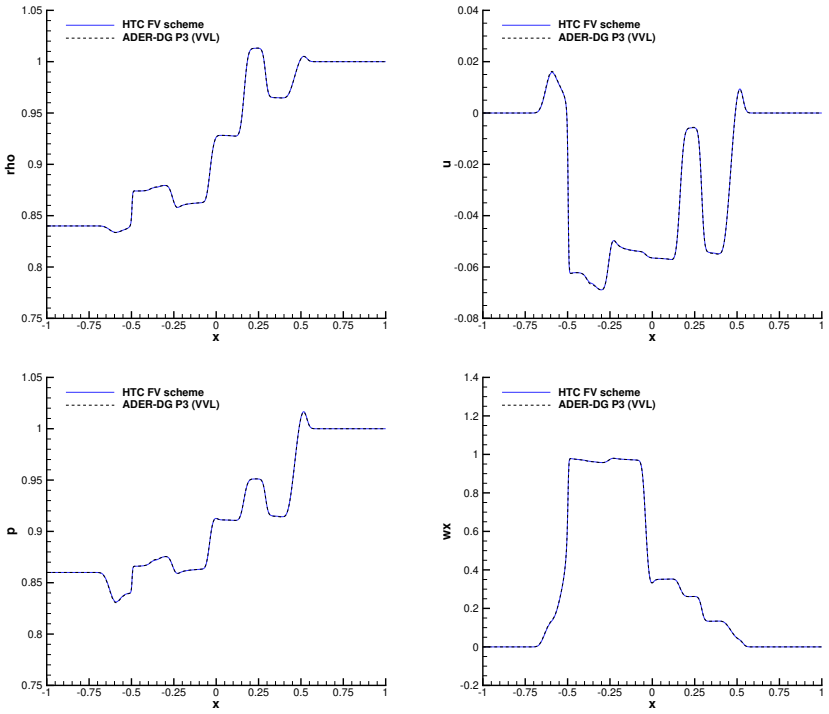

Fig. 1 Numerical solutions obtained at time $t = 0.3$ for the homogeneous Riemann problem RP1 without relaxation source terms using the new HTC finite volume scheme and the high order ADER-DG scheme ($N = 3$) applied to the vanishing viscosity limit (VVL) of the SHTC model ($\epsilon = 5 \cdot 10^{-4}$). From top left to bottom right: Mixture density ρ, mixture velocity v_1, mixture pressure p and relative velocity w_1.

for RP1 and RP2 are displayed in Figures 3 and 4 respectively. Overall the results computed with the new HTC and the ADER-DG VVL scheme match the Baer-Nunziato model in the stiff heat relaxation limit. Note that the ADER-DG VVL method uses a viscosity of $\epsilon = 2 \cdot 10^{-5}$ for RP1 and $\epsilon = 10^{-4}$ for RP2. This, together with the chosen relaxation rate τ, explains the deviations of the ADER-DG VVL approach from the solutions obtained with the Baer-Nunziato model, taking into account the distance to the relaxation limit. Since the HTC scheme does not need the additional viscosity ϵ, it captures accurately the waves that are present in the Baer-Nunziato model and reproduces the correct wave speeds for both considered Riemann problems.

5.3 Circular explosion problem

To complete the study of Riemann Problems for the two-fluid model (3), we consider RP1 in a radial set up with radius $r = \sqrt{x^2 + y^2}$ on the computational

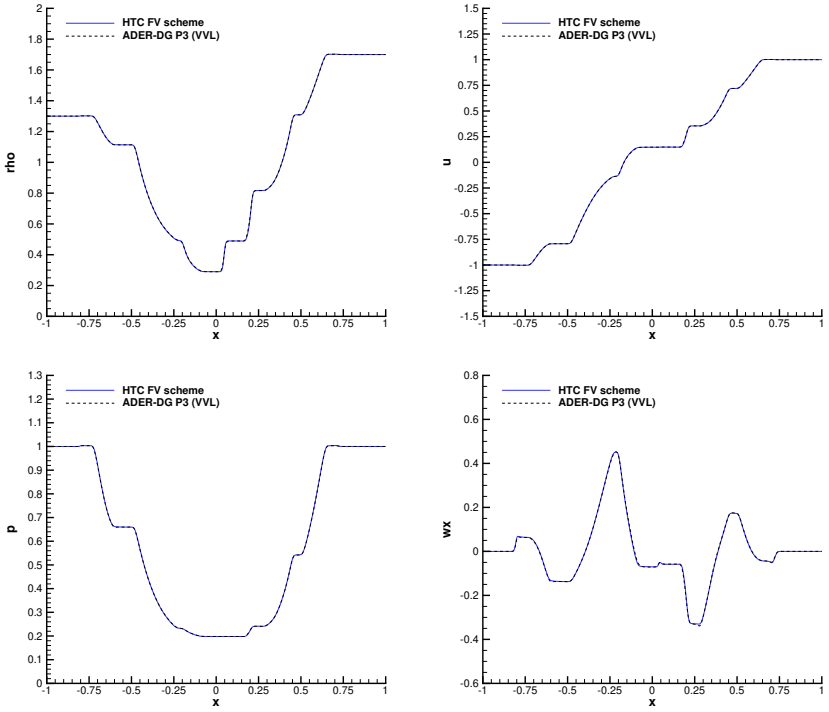

Fig. 2 Numerical solutions obtained at time $t = 0.3$ for the homogeneous Riemann problem RP2 without relaxation source terms using the new HTC finite volume scheme and the high order ADER-DG scheme ($N = 3$) applied to the vanishing viscosity limit (VVL) of the SHTC model ($\epsilon = 1 \cdot 10^{-4}$). From top left to bottom right: Mixture density ρ, mixture velocity v_1, mixture pressure p and relative velocity w_1.

domain $[-1, 1]^2$ where the left state is applied for $r < r_0$ and the right state for $r \geq r_0$ with the interface placed at $r_0 = 0.6$. The difference to the one dimensional RP1 in Section 5.2 consists of the presence of the lift forces in the relative velocity equation of the SHTC two-fluid model (3) which reflect in the appearance of the additional non-conservative terms (16) in the corresponding Baer-Nunziato formulation (12). These lift forces are only triggered in the multi-dimensional case and vanish in the one-dimensional set-up. In Figure 6 we compare the results of the new HTC scheme in the stiff relaxation limit with $\varepsilon = 5 \cdot 10^{-5}$ on a 1536×1536 mesh against the Baer-Nunziato limit system solved with the ADER-DG scheme with $N = 3$ and 512^2 elements. For ease of comparison, we plot the cut along the x-axis on the domain $[0, 1]$ since the test results in symmetric wave propagation. As we can see, the results of the SHTC model in the stiff relaxation limit obtained with the new HTC scheme match with the solution of Baer-Nunziato limit system. As previously observed in Figure 3, we can see marginal differences between the two graphs, which can be again explained with the distance to the actual limit since $\tau = \mathcal{O}(10^{-5})$

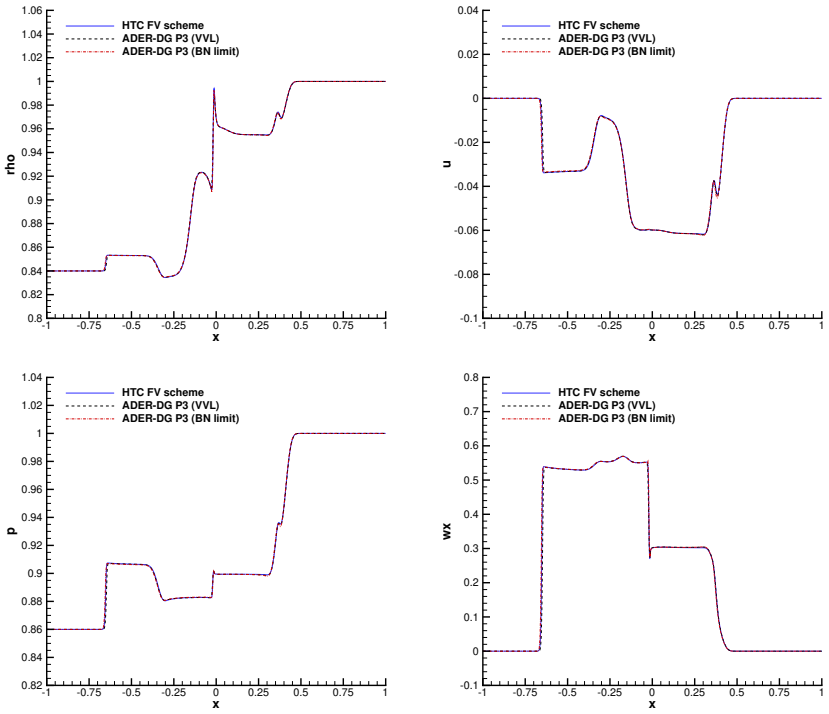

Fig. 3 Numerical solutions obtained at time $t = 0.3$ for the homogeneous Riemann problem RP1 in the stiff relaxation limit ($A^1 = A^2 = 400$, $\kappa_1 = \kappa_2 = 2 \cdot 10^{-3}$) using the new HTC finite volume scheme and the high order ADER-DG scheme ($N = 3$) applied to the vanishing viscosity limit (VVL) of the SHTC model ($\epsilon = 2 \cdot 10^{-5}$). From top left to bottom right: Mixture density ρ, mixture velocity v_1, mixture pressure p and relative velocity w_1.

and the viscosity of the HTC scheme. More importantly, both solutions match in the wave speeds and positions and therefore the results obtained with the HTC scheme based on the SHTC equations (3) show good agreement and verify numerically the stiff heat relaxation limit given by the Baer-Nunziato model (12).

5.4 Two-fluid Kelvin-Helmholtz instabilities

The next test case regards the simulation of two-fluid Kelvin-Helmholtz instabilities on a computational domain of $[-0.5, 0.5] \times [-1, 1]$ with periodic boundary conditions in x- and y-direction. The initial set-up is an adaption of the standard Kelvin-Helmholtz instability test case for the Euler equations in a compressible regime to the two-fluid case where the jump in the densities at

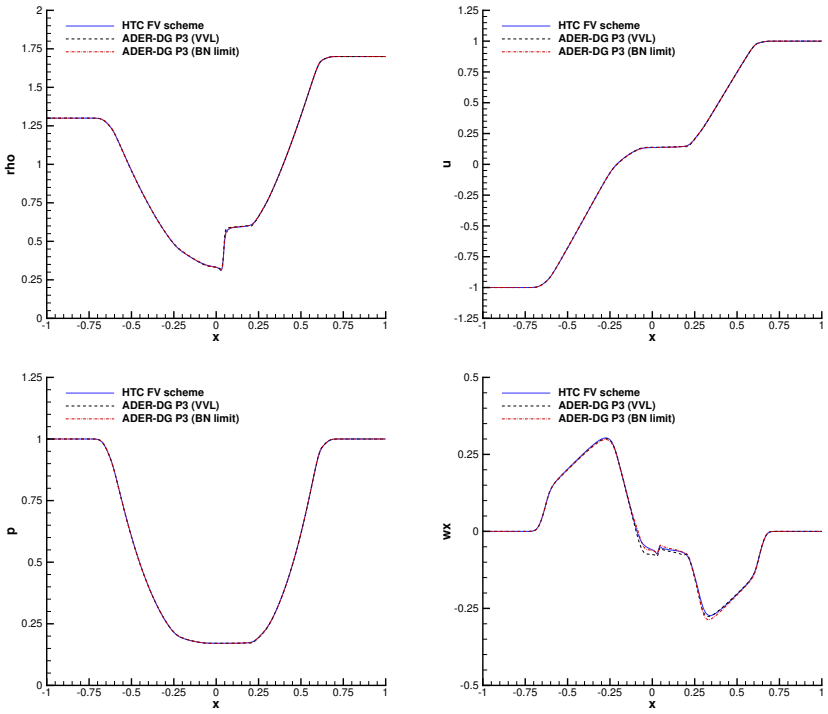

Fig. 4 Numerical solutions obtained at time $t = 0.3$ for the homogeneous Riemann problem RP2 in the stiff relaxation limit ($A^1 = A^2 = 400$, $\kappa_1 = \kappa_2 = 2 \cdot 10^{-3}$) using the new HTC finite volume scheme and the high order ADER-DG scheme ($N = 3$) applied to the vanishing viscosity limit (VVL) of the SHTC model ($\epsilon = 1 \cdot 10^{-4}$). From top left to bottom right: Mixture density ρ, mixture velocity v_1, mixture pressure p and relative velocity w_1.

the interface is modeled by a rapid change in the volume fraction given by

$$\alpha^1 = \begin{cases} 0.5 + 0.25 \tanh\left(25\left(y + 0.5\right)\right) & \text{if} \quad y < 0 \\ 0.5 - 0.25 \tanh\left(25\left(y - 0.5\right)\right) & \text{if} \quad y \geq 0 \end{cases}. \tag{58}$$

Therefore, the initial densities are constant on the whole domain and given by $\rho^1 = 1$ and $\rho^2 = 2$. The two considered materials are described as in the previous test cases by $\gamma^1 = 1.4$ and $\gamma^2 = 2$ where we set here $c_v^1 = c_v^2 = 4$. To highlight the instabilities generated by the shear flow, the pressure for both phases coincides and is set to $p^1 = p^2 = 100/\gamma^1$ which yields a reference Mach number regime of $\mathcal{O}(10^{-1})$ for both phases. The thermal impulses are initially set to zero, i.e. $\mathbf{j}^1 = 0$, $\mathbf{j}^2 = 0$ and we consider a moderate influence setting $A^1 = A^2 = 1$ if no relation source terms are present. For the stiff relaxation limit, we consider $A^1 = A^2 = 100$ and $\kappa^1 = \kappa^2 = 2 \cdot 10^{-3}$. The velocities of

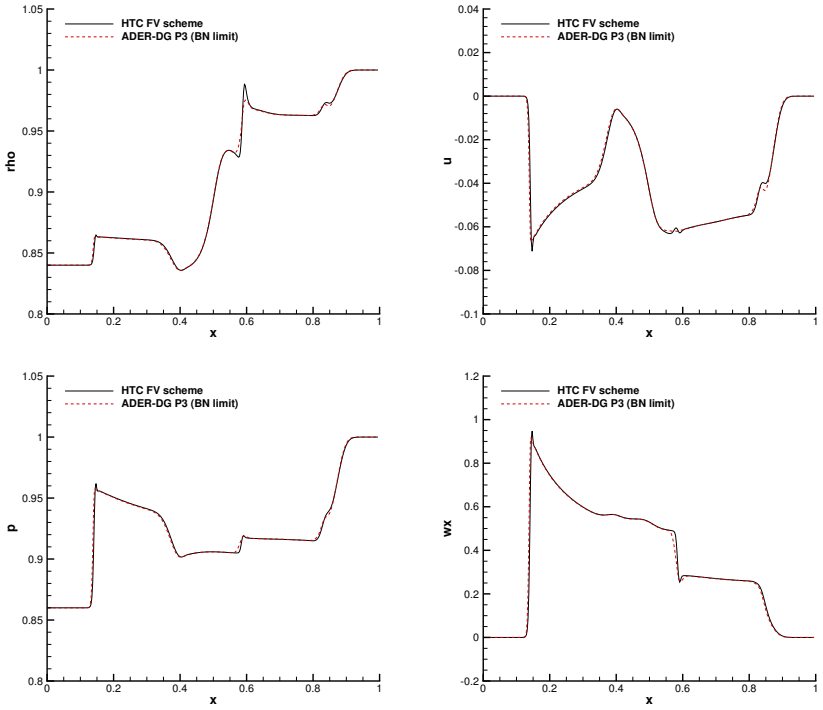

Fig. 5 Numerical solutions obtained at time $t = 0.2$ for the circular explosion problem based on RP1 in the stiff relaxation limit of the SHTC model ($A^1 = A^2 = 400$, $\kappa_1 = \kappa_2 = 2 \cdot 10^{-3}$) using the new HTC finite volume scheme and the high order ADER-DG scheme ($N = 3$) applied to the parabolic Baer-Nunziato-type limit model. From top left to bottom right: Mixture density ρ, mixture velocity v_1, mixture pressure p and relative velocity w_1.

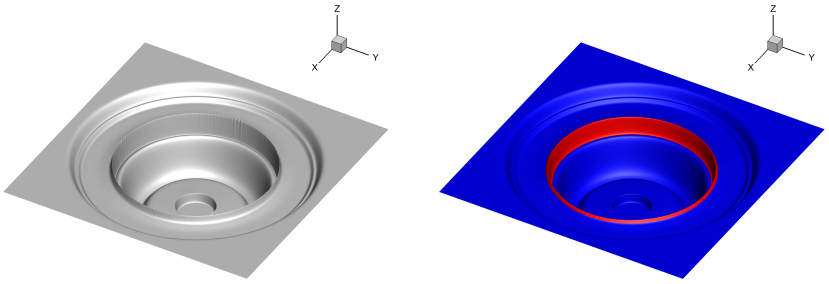

Fig. 6 3D view of the mixture density profile obtained at time $t = 0.2$ for the circular explosion problem. Left: new HTC finite volume scheme applied to the SHTC model. Right: ADER-DG scheme ($N = 3$) applied to the parabolic Baer-Nunziato-type limit model (red cells are troubled cells, where the *a posteriori* subcell FV limiter has been applied).

both phases coincide initially and are set in the x component to

$$v_1^1 = v_2^1 = \begin{cases} +0.5 \tanh\left(25\left(y+0.5\right)\right) & \text{if} \quad y < 0 \\ -0.5 \tanh\left(25\left(y-0.5\right)\right) & \text{if} \quad y \geq 0 \end{cases}. \tag{59}$$

To trigger the instablities, a small perturbation is applied in the y component given by

$$v_1^2 = v_2^2 = \begin{cases} -10^{-2} \sin\left(2\pi x\right) \sin\left(2\pi(y+0.5)\right) & \text{if} \quad y < 0 \\ +10^{-2} \sin\left(2\pi x\right) \sin\left(2\pi(y-0.5)\right) & \text{if} \quad y \geq 0 \end{cases}. \tag{60}$$

We first run the HTC FV scheme on the homogeneous SHTC model, i.e. without algebraic relaxation source terms up to a final time $t = 8$ and $\epsilon = 2.5 \cdot 10^{-5}$ on a 1024×2048 mesh which ensures the same resolution in x- and y-direction. The snapshots at times $t \in \{3, 4, 5, 6, 7, 8\}$ for the volume fraction α^1 which is a passively transported quantity is depicted in Figure 8. We can observe the formation of the characteristic instabilities at the interface between the two phases and the subsequent mixing of the two considered agents. In Figure 7 we display the results for the same set up in the stiff relaxation limit. However, the presence of the heat related relaxation terms and the increased influence of the thermal impulses on the internal energy only marginally affects the evolution of the flow since, initially zero, they are generated by a change of the temperatures, which are initially constant. We would like to emphasize that in both cases, the new HTC scheme is able to produce well resolved vortices with a good separation of the two phases.

5.5 Influence of the lift forces

One of the main differences between the SHTC two-fluid model (3) with the standard Baer-Nunziato approach to describe two-fluid flows consists in the lift forces (16). In the next test case we numerically study their influence on the solution using the ADER-DG scheme. As they are terms involving the curl of the relative velocity, they are present only when considering two or higher dimensional problems. Therefore we consider the vortex introduced in Section 5.1 as initial condition and compare the solutions obtained with the SHTC model (3) and the Baer-Nunziato model (12) with and without lift forces at time $T_f = 1$ in the stiff heat relaxation limit using $A^1 = A^2 = 1000$ and $\kappa^1 = \kappa^2 = 10^{-3}$ resulting in $\tau = \mathcal{O}(10^{-7})$. Since the vortex is smooth, we set $\epsilon = 0$. Therefore no additional viscosity is introduced by the ADER-DG VVL approach and we solve the full SHTC system without the green viscosity terms comparing directly the influence of the lift forces within the same numerical scheme.

In Figure 9, the results are shown along the x-axis for the mixture density, pressure, velocity and relative velocity, the latter two in the y-component. Note that the vortex is almost an exact solution, since τ is very small, to both the SHTC as well as the Baer-Nunziato system with lift forces thus the solution

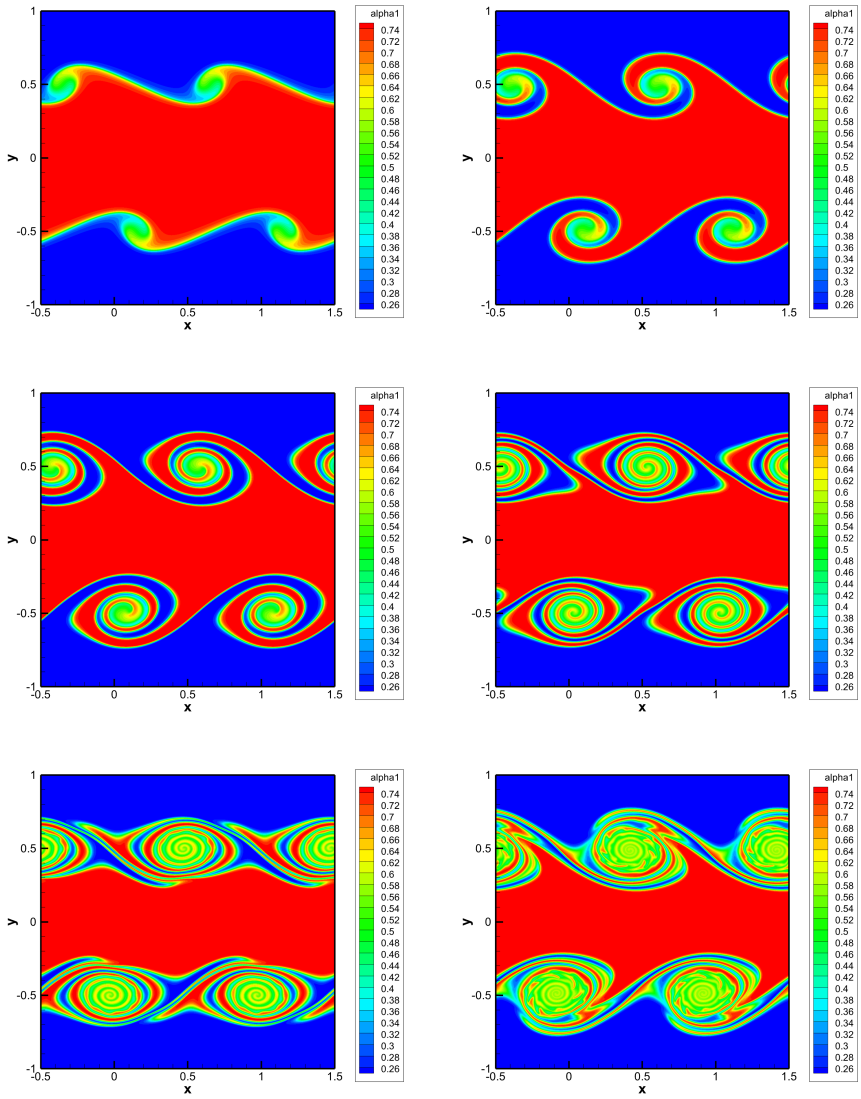

Fig. 7 Two-fluid Kelvin-Helmholtz instability: numerical solution obtained with the new HTC finite volume scheme at times $t \in \{3, 4, 5, 6, 7, 8\}$ for the *homogeneous* SHTC model without algebraic relaxation source terms. The employed mesh resolution was 1024×2048 elements and the artificial viscosity coefficient was set to $\epsilon = 2 \cdot 10^{-5}$.

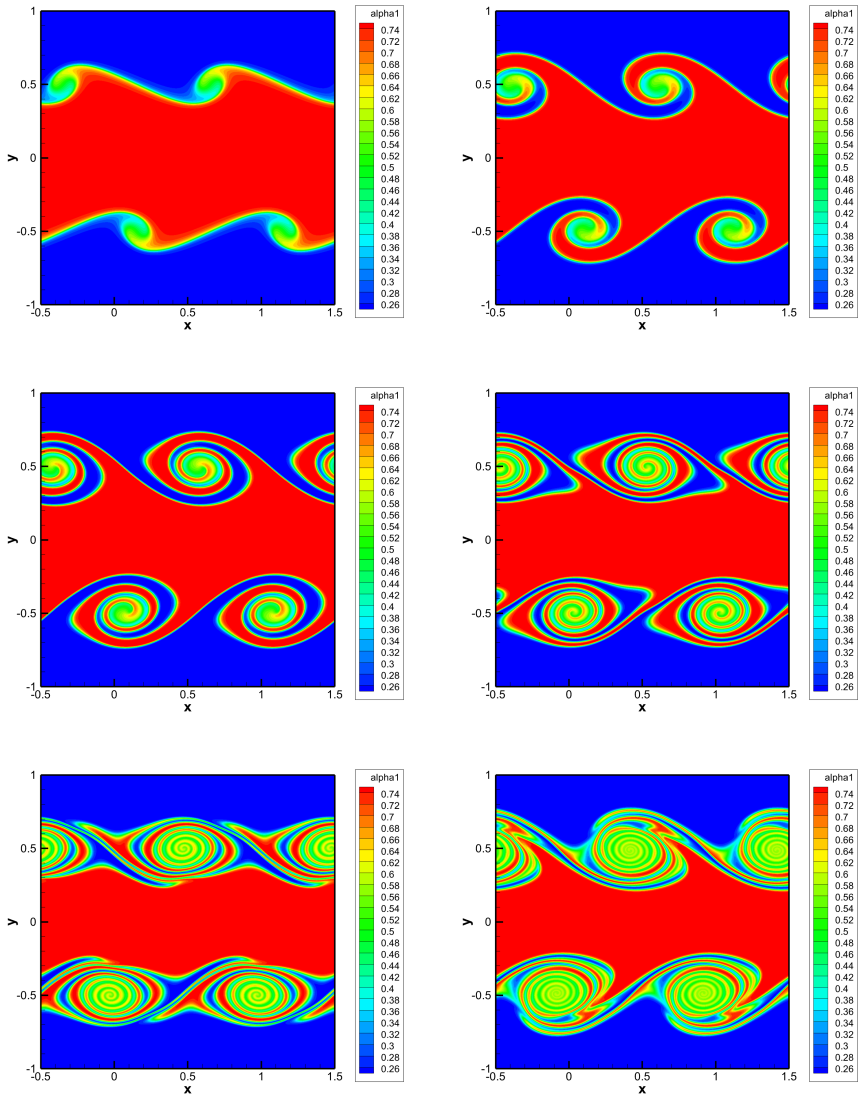

Fig. 8 Two-fluid Kelvin-Helmholtz instability: numerical solution obtained with the new HTC finite volume scheme at times $t \in \{3, 4, 5, 6, 7, 8\}$ for the SHTC model in the stiff relaxation limit ($A^1 = A^2 = 100$, $\kappa^1 = \kappa^2 = 2 \cdot 10^{-3}$). The employed mesh resolution was 1024×2048 elements and the artificial viscosity coefficient was set to $\epsilon = 2 \cdot 10^{-5}$.

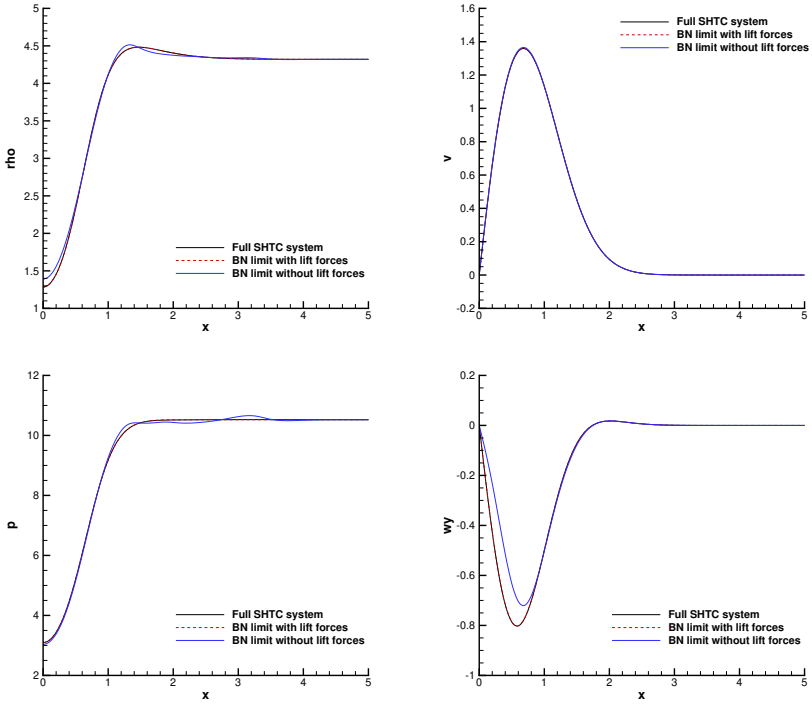

Fig. 9 Numerical solution obtained at time $t = 1.0$ for the vortex problem solved in the stiff relaxation limit of the SHTC model ($A^1 = A^2 = 1000$, $\kappa_1 = \kappa_2 = 1 \cdot 10^{-3}$) using the high order ADER-DG scheme ($N = 3$) applied to the vanishing viscosity limit (VVL) of the SHTC model ($\epsilon = 0$). Comparison with the Baer-Nunziato limit system with and without lift forces. From top left to bottom right: Mixture density ρ, mixture velocity v_2, mixture pressure p and relative velocity w_2.

of the SHTC and Baer-Nunziato with lift forces match perfectly. Switching off the lift forces in the Baer-Nunziato model significantly affects the relative velocity, as can be seen from Figure 9 as the lift forces directly act on the phase velocities increasing $\mathbf{v}^1$ and decreasing $\mathbf{v}^2$, since the relative velocity has a negative sign in this test case. Thus, the missing lift forces lead to a decrease in the relative velocities.

6 Conclusion

In this paper we have introduced a new thermodynamically compatible finite volume scheme for the symmetric hyperbolic and thermodynamically compressible (SHTC) two-fluid model of Romenski *et al.* [66,65] that is endowed with two entropy inequalities. The new method is able to discretize the two entropy inequalities directly and obtains total energy conservation as a mere consequence of the thermodynamically compatible discretization of all other

equations. The thermodynamically compatible numerical flux is based on the seminal ideas of Abgrall [2,9,8], which was subsequently generalized and applied to SHTC systems in [3,18]. Compared to previous thermodynamically compatible finite volume schemes the new approach forwarded in this paper does not require the computation of any path integral but is totally general and can be applied to arbitrary overdetermined hyperbolic and thermodynamically compatible systems of the form (17) that admit an extra conservation law of the type (18). The proposed HTC FV schemes satisfy two discrete entropy inequalities and are provably nonlinearly stable in the energy norm. In this paper we furthermore consider arbitrary high order accurate discontinuous Galerkin (DG) schemes applied to the vanishing viscosity limit of the overdetermined system. In this case, no particular care is taken to satisfy (18) exactly at the discrete level, apart from the mere resolution of all flow features. In the numerical results section we have clearly shown that the schemes proposed in this paper achieve their designed order of accuracy and that in the stiff relaxation limit the numerical solution tends to the asymptotically reduced Baer-Nunziato (BN) limit system with lift forces. The influence of the lift forces has been studied separately, showing that their presence in the BN limit is necessary to achieve a good agreement with the underlying SHTC system.

Future work will concern the extension to more general multi-phase flows with more than two phases [64], the development of asymptotic-preserving semi-implicit all Mach number schemes [59,38,36,1,16,62,53] and the extension to HTC schemes that satisfy the non-homogeneous curl involution on the relative velocity exactly at the discrete level, see e.g. [14,16,33].

Acknowledgements

M.D. is member of the INdAM GNCS group and acknowledges the financial support received from the Italian Ministry of Education, University and Research (MIUR) in the frame of the PRIN 2017 project *Innovative numerical methods for evolutionary partial differential equations and applications* and via the Departments of Excellence Initiative 2018–2027 attributed to DICAM of the University of Trento (grant L. 232/2016). The authors would like to thank the Leibniz Rechenzentrum (LRZ) in Garching, Germany, for the access to SuperMUC-NG under project pr83no. A. T. has been partially supported by the Gutenberg Research College, JGU Mainz.

Conflict of Interest

The authors declare that they have no conflict of interest.

Data availability

The data can be obtained from the authors on reasonable request.

References

1. Abbate, E., Iollo, A., Puppo, G.: An asymptotic-preserving all-speed scheme for fluid dynamics and nonlinear elasticity. SIAM Journal on Scientific Computing **41**, A2850–A2879 (2019)
2. Abgrall, R.: A general framework to construct schemes satisfying additional conservation relations. Application to entropy conservative and entropy dissipative schemes. J. Comput. Phys. **372**, 640–666 (2018)
3. Abgrall, R., Busto, S., Dumbser, M.: A simple and general framework for the construction of thermodynamically compatible schemes for computational fluid and solid mechanics. Applied Mathematics and Computation **440**, 127629 (2023)
4. Abgrall, R., Karni, S.: Computations of Compressible Multifluids. J. Comput. Phys. **169**, 594–623 (2001)
5. Abgrall, R., Karni, S.: A comment on the computation of non-conservative products. J. Comput. Phys. **229**, 2759–2763 (2010)
6. Abgrall, R., Nkonga, B., Saurel, R.: Efficient numerical approximation of compressible multi-material flow for unstructured meshes. Computers and Fluids **32**, 571–605 (2003)
7. Abgrall, R., Nordström, J., Öffner, P., Tokareva, S.: Analysis of the SBP-SAT stabilization for finite element methods. I: Linear problems. Journal of Scientific Computing **85**(2), 28 (2020)
8. Abgrall, R., Nordström, R., Öffner, P., Tokareva, S.: Analysis of the SBP-SAT stabilization for finite element methods. Part II: Entropy Stability. Commun. Appl. Math. Comput. (2021). DOI 10.1007/s42967-020-00086-2
9. Abgrall, R., Öffner, P., Ranocha, H.: Reinterpretation and extension of entropy correction terms for residual distribution and discontinuous galerkin schemes: Application to structure preserving discretization. Journal of Computational Physics **453** (2022)
10. Abgrall, R., Saurel, R.: Discrete equations for physical and numerical compressible multiphase mixtures. J. Comput. Phys. **186**, 361–396 (2003)
11. Andrianov, N., Saurel, R., Warnecke, G.: A simple method for compressible multiphase mixtures and interfaces. Int. J. Numer. Methods Fluids **41**, 109–131 (2003)
12. Andrianov, N., Warnecke, G.: The Riemann problem for the Baer–Nunziato two-phase flow model. J. Comput. Phys. **212**, 434–464 (2004)
13. Baer, M., Nunziato, J.: A two-phase mixture theory for the deflagration-to-detonation transition (DDT) in reactive granular materials. J. Multiphase Flow **12**, 861–889 (1986)
14. Balsara, D., Käppeli, R., Boscheri, W., Dumbser, M.: Curl constraint-preserving reconstruction and the guidance it gives for mimetic scheme design. Communications in Applied Mathematics and Computational Science (2023). DOI 10.1007/s42967-021-00160-3
15. Boscheri, W., Dumbser, M.: Arbitrary-Lagrangian-Eulerian discontinuous Galerkin schemes with a posteriori subcell finite volume limiting on moving unstructured meshes. J. Comput. Phys. **346**, 449 – 479 (2017)
16. Boscheri, W., Dumbser, M., Ioriatti, M., Peshkov, I., Romenski, E.: A structure-preserving staggered semi-implicit finite volume scheme for continuum mechanics. J. Comput. Phys. **424**, 109866 (2021)
17. Busto, S., Chiocchetti, S., Dumbser, M., Gaburro, E., Peshkov, I.: High order ADER schemes for continuum mechanics. Frontiers in Physics **8**, 32 (2020)
18. Busto, S., Dumbser, M.: A new class of efficient finite volume schemes for overdetermined thermodynamically compatible hyperbolic systems. Communications in Applied Mathematics and Computational Science (2023)
19. Busto, S., Dumbser, M.: A new thermodynamically compatible finite volume scheme for magnetohydrodynamics. SIAM Journal on Numerical Analysis **61**, 343–364 (2023)
20. Busto, S., Dumbser, M., Gavrilyuk, S., Ivanova, K.: On thermodynamically compatible finite volume methods and path-conservative ADER discontinuous Galerkin schemes for turbulent shallow water flows. J. Sci. Comput. **88**, 28 (2021)
21. Busto, S., Dumbser, M., Peshkov, I., Romenski, E.: On thermodynamically compatible finite volume schemes for continuum mechanics. SIAM Journal on Scientific Computing **44**, A1723–A1751 (2022)

22. Busto, S., Toro, E., Vázquez-Cendón, E.: Design and analysis of ADER-type schemes for model advection–diffusion–reaction equations. J. Comput. Phys. **327**, 553–575 (2016)
23. Castro, M., Gallardo, J., López, J., Parés, C.: Well-balanced high order extensions of godunov's method for semilinear balance laws. SIAM J. Numer. Anal. **46**, 1012–1039 (2008)
24. Castro, M., Gallardo, J., Parés, C.: High-order finite volume schemes based on reconstruction of states for solving hyperbolic systems with nonconservative products. Applications to shallow-water systems. Math. Comput. **75**, 1103–1134 (2006)
25. Castro, M., LeFloch, P., Muñoz-Ruiz, M., Parés, C.: Why many theories of shock waves are necessary: Convergence error in formally path-consistent schemes. J. Comput. Phys. **227**, 8107–8129 (2008)
26. Chertock, A., Degond, P., Neusser, J.: An asymptotic-preserving method for a relaxation of the navier–stokes–korteweg equations. Journal of Computational Physics **335**, 387–403 (2017)
27. Chiocchetti, S., Dumbser, M.: An exactly curl-free staggered semi-implicit finite volume scheme for a first order hyperbolic model of viscous flow with surface tension. Journal of Scientific Computing **94**, 24 (2023)
28. Chiocchetti, S., Peshkov, I., Gavrilyuk, S., Dumbser, M.: High order ADER schemes and GLM curl cleaning for a first order hyperbolic formulation of compressible flow with surface tension. Journal of Computational Physics **426**, 109898 (2021)
29. Clain, S., Diot, S., Loubère, R.: A high–order finite volume method for systems of conservation laws - Multi–dimensional Optimal Order Detection (MOOD). J. Comput. Phys. **230**, 4028–4050 (2011)
30. Clain, S., Diot, S., Loubère, R.: A high-order finite volume method for systems of conservation laws - Multi-dimensional Optimal Order Detection (MOOD). J. Comput. Phys. **230**, 4028 – 4050 (2011)
31. De Lorenzo, M., Pelanti, M., Lafon, P.: Hllc-type and path-conservative schemes for a single–velocity six-equation two-phase flow model: A comparative study. Appl. Math. Comput. **333**, 95–117 (2018)
32. Dhaouadi, F., Dumbser, M.: A first order hyperbolic reformulation of the navier-stokes-korteweg system based on the gpr model and an augmented lagrangian approach. Journal of Computational Physics **470**, 111544 (2022)
33. Dhaouadi, F., Dumbser, M.: A structure-preserving finite volume scheme for a hyperbolic reformulation of the Navier-Stokes-Korteweg equations. Mathematics **11**, 876 (2023). DOI 0.3390/math11040876
34. Diehl, D., Kremser, J., Kröner, D., Rohde, C.: Numerical solution of Navier–Stokes–Korteweg systems by Local Discontinuous Galerkin methods in multiple space dimensions. Appl. Math. Comput. **272**, 309–335 (2016)
35. Diot, S., Clain, S., Loubère, R.: Improved detection criteria for the multi-dimensional optimal order detection (MOOD) on unstructured meshes with very high-order polynomials. J. Comput. Phys. **64**, 43 – 63 (2012)
36. Dumbser, M., Balsara, D., Tavelli, M., Fambri, F.: A divergence-free semi-implicit finite volume scheme for ideal, viscous and resistive magnetohydrodynamics. International Journal for Numerical Methods in Fluids **89**, 16–42 (2019)
37. Dumbser, M., Balsara, D., Toro, E., Munz, C.: A unified framework for the construction of one–step finite–volume and discontinuous Galerkin schemes. J. Comput. Phys. **227**, 8209–8253 (2008)
38. Dumbser, M., Casulli, V.: A conservative, weakly nonlinear semi-implicit finite volume method for the compressible Navier-Stokes equations with general equation of state. Applied Mathematics and Computation **272**, 479–497 (2016)
39. Dumbser, M., Enaux, C., Toro, E.: Finite volume schemes of very high order of accuracy for stiff hyperbolic balance laws. J. Comput. Phys. **227**, 3971–4001 (2008)
40. Dumbser, M., Hidalgo, A., Castro, M., Parés, C., Toro, E.: FORCE schemes on unstructured meshes II: Non–conservative hyperbolic systems. Computer Methods in Applied Mechanics and Engineering **199**, 625–647 (2010)
41. Dumbser, M., Loubère, R.: A simple robust and accurate a posteriori sub-cell finite volume limiter for the discontinuous Galerkin method on unstructured meshes. J. Comput. Phys. **319**, 163–199 (2016)

42. Dumbser, M., Peshkov, I., Romenski, E., Zanotti, O.: High order ADER schemes for a unified first order hyperbolic formulation of continuum mechanics: Viscous heat–conducting fluids and elastic solids. J. Comput. Phys. **314**, 824–862 (2016)
43. Dumbser, M., Zanotti, O., Loubère, R., Diot, S.: A posteriori subcell limiting of the discontinuous Galerkin finite element method for hyperbolic conservation laws. J. Comput. Phys. **278**, 47–75 (2014)
44. Favrie, N., Gavrilyuk, S.: Diffuse interface model for compressible fluid - Compressible elastic-plastic solid interaction. J. Comput. Phys. **231**, 2695–2723 (2012)
45. Favrie, N., Gavrilyuk, S., R.Saurel: Solid–fluid diffuse interface model in cases of extreme deformations. J. Comput. Phys. **228**, 6037–6077 (2009)
46. Gassner, G., Lörcher, F., Munz, C.: A contribution to the construction of diffusion fluxes for finite volume and discontinuous Galerkin schemes. J. Comput. Phys. **224**, 1049–1063 (2007)
47. Gavrilyuk, S., Ivanova, K., Favrie, N.: Multi-dimensional shear shallow water flows: Problems and solutions. J. Comput. Phys. **366**, 252–280 (2018)
48. Godunov, S.: An interesting class of quasilinear systems. Dokl. Akad. Nauk SSSR **139(3)**, 521–523 (1961)
49. Godunov, S.: Symmetric form of the equations of magnetohydrodynamics. Numerical Methods for Mechanics of Continuous Media **3**(1), 26–31 (1972)
50. Godunov, S., Romenski, E.: Elements of continuum mechanics and conservation laws. Kluwer Academic/Plenum Publishers (2003)
51. Hitz, T., Keim, J., Munz, C., Rohde, C.: A parabolic relaxation model for the navier-stokes-korteweg equations. Journal of Computational Physics **421**, 109714 (2020)
52. Kapila, A., Menikoff, R., Bdzil, J., Son, S., Stewart, D.: Two-phase modelling of DDT in granular materials: reduced equations. Physics of Fluids **13**, 3002–3024 (2001)
53. Lukácová-Medvidóvá, M., Puppo, G., Thomann, A.: An all Mach number finite volume method for isentropic two-phase flow. Journal of Numerical Mathematics (2023). In press. doi: https://doi.org/10.1515/jnma-2022-0015
54. Maso, G.D., LeFloch, P., Murat, F.: Definition and weak stability of nonconservative products. J. Math. Pures Appl. **74**, 483–548 (1995)
55. Muñoz, M., Parés, C.: Godunov method for nonconservative hyperbolic systems. Mathematical Modelling and Numerical Analysis **41**, 169–185 (2007)
56. Ndanou, S., Favrie, N., Gavrilyuk, S.: Multi-solid and multi-fluid diffuse interface model: Applications to dynamic fracture and fragmentation. J. Comput. Phys. **295**, 523–555 (2015)
57. Neusser, J., Rohde, C., Schleper, V.: Relaxation of the navier–stokes–korteweg equations for compressible two-phase flow with phase transition. International Journal for Numerical Methods in Fluids **79**(12), 615–639 (2015)
58. Parés, C.: Numerical methods for nonconservative hyperbolic systems: a theoretical framework. SIAM J. Numer. Anal. **44**, 300–321 (2006)
59. Park, J., Munz, C.: Multiple pressure variables methods for fluid flow at all mach numbers. International Journal for Numerical Methods in Fluids **49**, 905–931 (2005)
60. Pelanti, M., Leveque, R.: High-resolution finite volume methods for dusty gas jets and plumes. SIAM J. Sci. Comput. **28**(4), 1335–1360 (2006)
61. Pelanti, M., Shyue, K.: A numerical model for multiphase liquid–vapor–gas flows with interfaces and cavitation. International Journal of Multiphase Flow **113**, 208–230 (2019)
62. Re, B., Abgrall, R.: A pressure-based method for weakly compressible two-phase flows under a Baer-–Nunziato type model with generic equations of state and pressure and velocity disequilibrium. International Journal on Numerical Methods in Fluids **94**(8), 1183–1232 (2022)
63. Romenski, E.: Hyperbolic systems of thermodynamically compatible conservation laws in continuum mechanics. Math. Comput. Modell. **28(10)**, 115–130 (1998)
64. Romenski, E., Belozerov, A., Peshkov, I.: Conservative formulation for compressible multiphase flows. Quarterly of Applied Mathematics **74**, 113–136 (2016)
65. Romenski, E., Drikakis, D., Toro, E.: Conservative models and numerical methods for compressible two-phase flow. J. Sci. Comput. **42**, 68–95 (2010)
66. Romenski, E., Resnyansky, A., Toro, E.: Conservative hyperbolic formulation for compressible two-phase flow with different phase pressures and temperatures. Q. Appl. Math. **65**, 259–279 (2007)

67. Saurel, R., Abgrall, R.: A multiphase Godunov method for compressible multifluid and multiphase flows. J. Comput. Phys. **150**, 425–467 (1999)
68. Scannapieco, A., Cheng, B.: A multifluid interpenetration mix model. Physics Letters A **299**(1), 49–64 (2002)
69. Schmidmayer, K., Petitpas, F., Daniel, E., Favrie, N., Gavrilyuk, S.: A model and numerical method for compressible flows with capillary effects. Journal of Computational Physics **334**, 468–496 (2017)
70. Schwendeman, D., Wahle, C., Kapila, A.: The Riemann problem and a high-resolution Godunov method for a model of compressible two-phase flow. J. Comput. Phys. **212**, 490–526 (2006)
71. Thein, F., Romenski, E., Dumbser, M.: Exact and numerical solutions of the Riemann problem for a conservative model of compressible two-phase flows. Journal of Scientific Computing **93**, 83 (2022)
72. Titarev, V., Toro, E.: ADER: Arbitrary high order Godunov approach. J. Sci. Comput. **17**(1-4), 609–618 (2002)
73. Titarev, V., Toro, E.: ADER schemes for three-dimensional nonlinear hyperbolic systems. J. Comput. Phys. **204**, 715–736 (2005)
74. Toro, E.F.: Riemann solvers and numerical methods for fluid dynamics, Second Edition. Springer–Verlag (1999)
75. Toro, E.F., Titarev, V.A.: Derivative Riemann solvers for systems of conservation laws and ADER methods. J. Comput. Phys. **212**(1), 150–165 (2006)
76. Zanotti, O., Fambri, F., Dumbser, M., Hidalgo, A.: Space–time adaptive ADER discontinuous Galerkin finite element schemes with a posteriori sub–cell finite volume limiting. Computers and Fluids **118**, 204–224 (2015)
77. Zanotti, O., Fambri, F., Dumbser, M., Hidalgo, A.: Space-time adaptive ADER discontinuous Galerkin finite element schemes with a posteriori sub-cell finite volume limiting. Computers and Fluids **118**, 204 – 224 (2015)

A Polar coordinate representation of the two-fluid model

We consider a continuous solution of the homogeneous (black) part of system (3). Let the Cartesian coordinates in 2D be denoted by $x = (x_1.x_2)$. Then we can define the polar coordinates in terms of radius r and angle θ as

$$x_1 = r\cos(\theta). \quad x_2 = r\sin(\theta). \tag{61}$$

The velocity and thermal impuls vectors are defined by

$$v_1 = v_r\cos(\theta) - v_\theta\sin(\theta), \qquad v_2 = v_r\cos(\theta) + v_\theta\sin(\theta), \tag{62a}$$
$$w_1 = w_r\cos(\theta) - w_\theta\sin(\theta), \qquad w_2 = w_r\cos(\theta) + w_\theta\sin(\theta), \tag{62b}$$
$$j_1^1 = j_r^1\cos(\theta) - j_\theta^1\sin(\theta), \qquad j_2^1 = j_r^1\cos(\theta) + j_\theta^1\sin(\theta), \tag{62c}$$
$$j_1^2 = j_r^2\cos(\theta) - j_\theta^2\sin(\theta), \qquad j_2^2 = j_r^2\cos(\theta) + j_\theta^2\sin(\theta). \tag{62d}$$

Using

$$\frac{\partial x_1}{\partial r} = \cos(\theta), \quad \frac{\partial x_1}{\partial \theta} = -\frac{\sin(\theta)}{r}, \quad \frac{\partial x_2}{\partial r} = \sin(\theta), \quad \frac{\partial x_1}{\partial \theta} = \frac{\cos(\theta)}{r}, \tag{63}$$

we obtain the following system in polar coordinates for

$$\mathbf{q} = (\alpha^1, \alpha^1\rho^1, \alpha^2\rho^2, \rho v_r, \rho v_\theta, \rho w_r, \rho w_\theta, \rho j_r^1, \rho j_\theta^1, \rho j_r^2, \rho j_\theta^2, \alpha^1\rho^1 s^1, \alpha^2\rho^2 s^2)^T \tag{64}$$

as follows

$$\frac{\partial \alpha^1}{\partial t} + \frac{v_r}{r}\frac{\partial}{\partial r}\left(r\alpha^1\right) + \frac{v_\theta}{r}\frac{\partial}{\partial \theta}\alpha^1 = 0, \tag{65a}$$
$$\frac{\partial (\alpha^1\rho^1)}{\partial t} + \frac{1}{r}\frac{\partial}{\partial r}\left(r\alpha^1\rho^1 v_r^1\right) + \frac{1}{r}\frac{\partial}{\partial \theta}\left(\alpha^1\rho^1 v_\theta^1\right) = 0, \tag{65b}$$

$$\frac{\partial(\alpha^2\rho^2)}{\partial t} + \frac{1}{r}\frac{\partial}{\partial r}\left(r\alpha^2\rho^2 v_r^2\right) + \frac{1}{r}\frac{\partial}{\partial \theta}\left(\alpha^2\rho^2 v_\theta^2\right) = 0, \tag{65c}$$

$$\begin{aligned}\frac{\partial(\rho v_r)}{\partial t} &+ \frac{1}{r}\frac{\partial}{\partial r}\left(r\left(\rho v_r^2 + \rho c^1(1-c^1)w_r w_r + p\right)\right)\\ &+ \frac{1}{r}\frac{\partial}{\partial \theta}\left(\rho v_r v_\theta + \rho c^1 c^2 w_r w_\theta\right) = \frac{\rho v_\theta^2 + \rho c^1(1-c^1)w_\theta^2 + p}{r},\end{aligned} \tag{65d}$$

$$\begin{aligned}\frac{\partial(\rho v_\theta)}{\partial t} &+ \frac{1}{r}\frac{\partial}{\partial r}\left(r\left(\rho v_r v_\theta + \rho c^1(1-c^1)w_r w_\theta\right)\right)\\ &+ \frac{1}{r}\frac{\partial}{\partial \theta}\left(\rho v_\theta^2 + p + \rho c^1(1-c^1)w_\theta^2\right) = -\frac{\rho v_r v_\theta + \rho c^1 c^2 w_r w_\theta}{r},\end{aligned} \tag{65e}$$

$$\begin{aligned}\frac{\partial w_r}{\partial t} &+ \frac{\partial}{\partial r}\left(v_r w_r + v_\theta w_\theta + (1-2c^1)\frac{w_r w_r + w_\theta w_\theta}{2} + \mu_1 - \mu_2\right)\\ &+ v_\theta\left(\frac{1}{r}\frac{\partial}{\partial \theta}w_r - \frac{1}{r}\frac{\partial}{\partial r}\left(r w_\theta\right)\right) = 0\end{aligned} \tag{65f}$$

$$\begin{aligned}\frac{\partial w_\theta}{\partial t} &+ \frac{1}{r}\frac{\partial}{\partial \theta}\left(v_r w_r + v_\theta w_\theta + (1-2c^1)\frac{w_r w_r + w_\theta w_\theta}{2} + \mu_1 - \mu_2\right)\\ &+ v_r\left(\frac{1}{r}\frac{\partial}{\partial r}\left(r w_\theta\right) - \frac{1}{r}\frac{\partial}{\partial \theta}w_r\right) = 0\end{aligned} \tag{65g}$$

$$\frac{\partial(\rho j_r^1)}{\partial t} + \frac{1}{r}\frac{\partial}{\partial r}\left(r\left(\rho j_r^1 v_r + T^1\right)\right) + \frac{1}{r}\frac{\partial}{\partial \theta}\left(\rho j_r^1 v_\theta\right) = \frac{\rho j_\theta^1 v_\theta + T^1}{r}, \tag{65h}$$

$$\frac{\partial(\rho j_\theta^1)}{\partial t} + \frac{1}{r}\frac{\partial}{\partial r}\left(r\left(\rho j_\theta^1 v_r\right)\right) + \frac{1}{r}\frac{\partial}{\partial \theta}\left(\rho j_\theta^1 v_\theta + T^1\right) = -\frac{\rho j_\theta^1 v_r}{r}, \tag{65i}$$

$$\frac{\partial(\rho j_r^2)}{\partial t} + \frac{1}{r}\frac{\partial}{\partial r}\left(r\left(\rho j_r^2 v_r + T^2\right)\right) + \frac{1}{r}\frac{\partial}{\partial \theta}\left(\rho j_r^2 v_\theta\right) = \frac{\rho j_\theta^2 v_\theta + T^2}{r}, \tag{65j}$$

$$\frac{\partial(\rho j_\theta^2)}{\partial t} + \frac{1}{r}\frac{\partial}{\partial r}\left(r\left(\rho j_\theta^2 v_r\right)\right) + \frac{1}{r}\frac{\partial}{\partial \theta}\left(\rho j_\theta^2 v_\theta + T^2\right) = -\frac{\rho j_\theta^2 v_r}{r}, \tag{65k}$$

$$\frac{\partial(\alpha^1\rho^1 s^1)}{\partial t} + \frac{1}{r}\frac{\partial}{\partial r}\left(r\left(\alpha^1\rho^1 s^1 v_r + A^1 j_r^1\right)\right) + \frac{1}{r}\frac{\partial}{\partial \theta}\left(\alpha^1\rho^1 s^1 v_\theta + A^1 j_\theta^1\right) = 0, \tag{65l}$$

$$\frac{\partial(\alpha^2\rho^2 s^2)}{\partial t} + \frac{1}{r}\frac{\partial}{\partial r}\left(r\left(\alpha^2\rho^2 s^2 v_r + A^2 j_r^2\right)\right) + \frac{1}{r}\frac{\partial}{\partial \theta}\left(\alpha^1\rho^2 s^2 v_\theta + A^2 j_\theta^2\right) = 0. \tag{65m}$$